
Quinn's Law of Fluid Dynamics Pressure-driven Fluid Flow Through Closed Conduits

Hubert Michael Quinn

Department of Research and Development, the Wrangler Group LLC, Brighton, USA

Email address:

hubert@wranglergroup.com

To cite this article:

Hubert M. Quinn. Quinn's Law of Fluid Dynamics Pressure-driven Fluid Flow Through Closed Conduits. *Fluid Mechanics*. Vol. 5, No. 2, 2019, pp. 39-71. doi: 10.11648/j.fm.20190502.12

Received: October 12, 2019; **Accepted:** December 11, 2019; **Published:** January 6, 2020

Abstract: In this paper we develop from first principles a unique law pertaining to the flow of fluids through closed conduits. This law, which we call "Quinn's Law", may be described as follows: When fluids are forced to flow through closed conduits under the driving force of a pressure gradient, there is a linear relationship between the fluid-drag normalized dimensionless pressure gradient, P_Q , and the normalized dimensionless fluid current, C_Q . The relationship is expressed mathematically as: $P_Q = k_1 + k_2 C_Q$. This *linear* relationship remains the same whether the conduit is filled with or devoid of solid obstacles. The law differentiates, however, between a *packed* and an *empty* conduit by virtue of the *tortuosity* of the fluid path, which is seamlessly accommodated within the normalization framework of the law itself. When movement of the fluid is very close to being at rest, i.e., very slow, this relationship has the unique minimum constant value of k_1 , and as the fluid acceleration increases, it varies with a slope of k_2 as a function of normalized fluid current. Quinn's Law is validated herein by applying it to the data from published classical studies of measured permeability in both packed and empty conduits, as well as to the data generated by home grown experiments performed in the author's own laboratory.

Keywords: Closed Conduits, Conduit Permeability, Friction Factor, Wall Effect, Boundary Layer, Turbulent, Flow Profile, Chaos

1. Introduction

The history of attempts to quantify a relationship between fluid flow in closed conduits (whether it be in a packed conduit or in an empty conduit) and the relevant variables governing that relationship dates back at least to the work of Darcy in 1856 [1]. Since that time, a host of models have been proposed with their accompanying array of equations, each of which has its own limitations and restrictions [2]. Accordingly, the scientific literature is replete with reports of experimental results aimed at trying to resolve the many discrepancies which litter the fluid dynamics landscape [3]. In fact, this field of study is in such disarray that there is no currently accepted theory of fluid dynamics from which one could derive an analytical solution to the supposed governing equation of fluid dynamics, the Navier-Stokes equation [4].

This author has devoted his entire career to doing fluid flow measurements, predominantly in packed beds relating to the field of HPLC (High Pressure Liquid Chromatography) [5, 6, 7, 8, 9, 10, 11, 12.]. Rather than nibbling at the fringes

of this complicated field of study by trying to manipulate one of the currently accepted theories, a completely *different* approach was developed. The subsequent model, which we refer to as the Quinn Fluid Flow Model (QFFM) took approximately 20 years to formulate, was developed from first principles, and is different from any other model currently extant. Most importantly, it is a universal theory which applies to all fluid flow embodiments, regardless of whether they contain particles and regardless of the regime of flow in which they are operated. Moreover, it has been validated by testing it against a host of generally accepted experimental data reported in the literature, as well as this author's own measurements.

The dimensional manifestation of the QFFM is a complex equation containing many independent and dependent variables and is the properly formatted version of the continuity equation for fluid flow in closed conduits. On the other hand, there is a dimensionless manifestation of the QFFM, which we refer to as Quinn's Law, which is a simple linear relationship between the reduced pressure gradient and

the reduced fluid flow current in a closed conduit. In contrast to the complicated alternatives that conventional theories of fluid dynamics have to offer, Quinn's Law is very simple. It has just two variable parameters. More importantly, and in contrast to conventional theories, it is valid over the entire range of the fluid flow regime, providing analytical solutions in laminar, transitional and fully turbulent ranges of fluid flow.

This author's development of the QFFM was born of the frustration experienced in trying to reconcile experimental data and textbook teachings relative to packed/empty conduit permeability. For instance, the chromatographic literature abounds with erroneous teachings: incorrect use of velocity frames [13]; the notion that the particle size is defined by permeability (14); violations of Continuity Laws [15, 16, 17.]; self-serving validations [18]. Likewise, the engineering literature is littered with similar errors: misapplication of porosity function [19]; erroneous derivation of the viscous constant [20]; "blind leading the blind" syndrome [21]; mathematicians using computers to produce mind-numbing computations, which purport to explain equations that have no connection to fluid flow parameters in the first place [22]; contradictory statements of facts [23]; etc.; etc. Moreover, both disciplines are especially guilty of neglecting the role of *kinetic* considerations in favor of focusing too much on the less complex *laminar* flow regime.

2. Methods

In order to underscore the importance of achieving a comprehensive understanding of the physics underlying our theoretical development, rather than just the mathematical framework, we want to introduce upfront the important novel concepts which are part of the development of our solution to the problem. In this way, we hope the reader will be focused more on where these concepts fit into the overall comprehensive understanding, rather than becoming embroiled in the mathematics, which, after all, is simply the gravel of which the roadway is made, and is not a critical component to a discussion of what is the destination.

2.1.1. *Q* - hypothetical Particles

This idea is a very simple one. It is a way of subdividing the free space in an empty conduit, using the same mathematics that we use to assign free space to solid particles in a packed conduit. We accomplish this by extending the existing framework of particle porosity for packed conduits containing solid particles to accommodate particles of free space (no solid skeleton) in an empty conduit. The resultant framework is a universe of two mathematical half-planes, each of which is the mirror image of the other. Of particular importance in this theoretical development, however, is that we manage to avoid the point of discontinuity which would otherwise arise as a consequence of the theory at the axis of symmetry between the two mathematical half-planes, since this would cause the mathematics and, consequently, the entire logic to implode at this location. We accomplish this

task by only using the absolute value of the particle fraction $[\text{abs}(1-\epsilon_0)]$ function, which is always finite, in our definition of the Hypothetical Q Channel (HQC) diameter, d_c , which forms the basis of the QFFM. In other words, we only use that portion of the theory which is valid in the real world. In addition, we are careful to manage our mathematical framework to incorporate the Conservation Laws into our HQC by a mechanism which reconciles particle diameter, d_p , and conduit external porosity, ϵ_0 .

2.1.2. *r_k*-the Fluid Drag Normalization Coefficient

The concept underlying this parameter is, arguably, the most important element of the entire QFFM theory. It is the exchange rate necessary to create a common "currency" between viscous and kinetic considerations dictated by the Laws of Nature. We use the value of the ratio of surface area to cross-sectional area of a spherical particle, r_h , i.e., 4, to define our control volume, $(4\pi r_h^3/3=268)$, making this value the common denominator which connects the control volume, surface area, cross sectional area and fluid drag. Accordingly, in our permeability model, this common denominator takes on the dual role of (a) being the radius of the obstacle responsible for the fluid friction due to viscous considerations, and, (b) at the same time, represents the hydraulic radius of the flow channel responsible for the fluid friction due to kinetic considerations. We exploit this feature in our theory by providing a mechanism for normalizing fluid resistance by either (1) surface area contact ($k_1=4\pi r_h^2/3=67$), or, (2) *reciprocal* channel circumference ($k_2=1/(2\pi r_h)=1/25$).

2.1.3. *δ*-the Porosity Normalization Coefficient

This parameter represents one of the cornerstones of our theory which allows us to accommodate both packed and empty conduits. It is a specific property of the flow embodiment under study. For instance, the *same* packed conduit with x number of particles will have a *different* value for δ , than the *same* conduit packed with y number of the *same* particles. Thus, a packed and an empty conduit will also have different δ values. Our δ parameter establishes in our theory (and is confirmed by our pressure drop measurements) that the pressure drop in the kinetic term of the permeability equation is inversely proportional to the 6th power of the conduit external porosity. By combining our parameter δ with the modified Reynolds number, R_{em} , we create a unique grouping of terms, our Q_N parameter, which we term fluid current. This parameter is the engine that drives the fluid velocity profile and, accordingly, reconciles all forms of flow.

2.1.4. *γ*-the Architectural Normalization Coefficient

This parameter is a rather obvious development to anyone who has experience in building physical structures from scratch, such as a house or barn or wall, all of which are made of building blocks of wood/bricks/stones and, accordingly, forms the basis for one's thinking when one builds a packed conduit from building blocks of particles (stones) within a fixed volume of free space, i.e. a conduit.

2.1.5. λ -the Wall Effect Normalization Coefficient of Fluid Current

This parameter is another cornerstone in our framework which aligns the physics of a packed and empty conduit, but only manifests in the kinetic term. It is also a specific property of the flow embodiment under study, and only changes as a function of the specific wall effect of a given packed conduit. In this case, however, the effect of the wall is transferred to the motion of the fluid, which is why we describe it as a component of fluid current. The rationale behind this parameter is fairly well documented in the main body of our paper, wherein we took advantage of Prandtl's concept of the boundary layer in formulating our definition of the primary wall effect [24].

2.1.6. τ -the Tortuosity Normalization Coefficient

We believe that tortuosity is primarily a function of channel architecture normalized for conduit external porosity. Accordingly, we have defined this parameter as another normalization coefficient which, again, only manifests in the kinetic term of the permeability equation. It compensates for the *different* flow paths which are generated within *different* packed conduits, as well as compensating for the *unique* flow path generated within *all* empty conduits.

2.1.7. The Harmonic Oscillator

Finally, everything comes together in our notion that fluid flow in closed conduits, whether packed with solid particles or empty, is a form of harmonic motion. Intuition tells us that we ought to imagine that the fluid going through a packed bed has to somehow double back upon itself. This idea led to the concept of Simple Harmonic Motion (SHM). Once having understood that SHM was the operating principle governing fluid flow in closed conduits, the connection to uniform circular motion became obvious. This led to the realization that when the speed of the fluid at the wall is zero, the velocity is not zero because the fluid is changing direction simultaneously. This was enough to establish the viscous friction factor as the underlying concept behind the harmonic oscillator algorithm. Once having done this, it was relatively easy to figure out what parameter was what, in the fluid motion, and make a one-to-one correspondence between the dimensionless fluid viscous friction factor parameters and the dimensional simple harmonic motion parameters, which, incidentally, is the reason why the particular units of measure in the SHM can be *arbitrary*, as long as they are *self-consistent*. More accurately stated, we incorporate the framework of damped-SHM to accommodate the impact of *conduit* wall friction and *fluid internal* friction, using both as damping coefficients on the overall motion of the fluid.

The concept of "fluid chaos", which permeates conventional wisdom, is rejected in our theory. The best way to think about it is to imagine oneself as a hunter in the mountains. The deer, which is the focus of our hunt, is perfectly camouflaged against the background of the hillside. Thus, the deer is invisible to the hunter, despite the fact that

the deer's body is located in free space in all three dimensions, i.e., it has location coordinates in the x, y and z planes. The reason why the deer is invisible to the hunter is that, relative to the hillside background, the hunter cannot differentiate between the deer and the underbrush. It is only when the deer changes its positional coordinates relative to the hill in the background that the hunter can see it i.e., when the deer starts running. Moreover, because the movement of the deer is not restricted in terms of free space on the mountainside, his "movement profile" can be erratic, uniform in a straight line (if he follows a road, for instance), or combinations of the above, all driven by the whim of the deer's instincts. However, it is never chaotic or unpredictable, in a scientific context, that is.

In our Hypothetical Q Channel model, the fluid is equivalent to the deer, i.e., it has positional coordinates in all three planes, but the fluid flow profile cannot be distinguished from the background of the channel because its positional coordinates are indistinguishable relative to the conduit wall or conduit center line. It is only when we view the fluid through the "scope" of the Q_N parameter (4th dimension), that its positional coordinates are changed relative to the background conduit wall/center line. In addition, when viewing the fluid profile through the Q_N scope, the Q_N crosshairs must be spaced closely enough together, relative to the size of T, the time constant of the fluid motion, to generate a comprehensive image of the flow profile, just as the crosshairs in the hunter's telescopic sight must be adjusted, commensurate with the overall size of the deer.

Additionally, and in contrast to the movement of the deer, the fluid movement in our HQC is restricted in free space because of its driving force, i.e., the pressure drop (ΔP). Furthermore, when we normalize the pressure drop for the length of the conduit, L, i.e., the pressure gradient ($\Delta P/L$), we restrict the movement of the fluid even further, i.e., to just the cross-section of the HQC. Thus, as the fluid moves over the cross-section, its current is influenced by the walls of the conduit, i.e., wall friction. Because of internal fluid friction, as its speed increases, the fluid flow profile loses its "arc of motion" and, ultimately, simply moves back and forth over the cross-section in a virtual straight line, i.e., "plug flow". Thus, cross-channel mixing is greatly enhanced by convection which is driven by the kinetic term in the permeability equation.

The Hypothetical Q Channel, of course, does not exist in the real world. However, the model allows us to imagine the fluid moving through the conduit and when we do, what we see is not disorganized or chaotic motion, but a structural pattern characterized by SHM, regardless of Reynolds number or any conduit or particle parameter. Accordingly, we suggest that "fluid chaos" is in the eye/mind of the beholder.

2.1.8. Conventional Permeability Equations

Finally, having started at the beginning of our development with fundamental definitions, we make our way systematically through the governing equations, in order to

arrive at the equation most useful to the practitioner of permeability. In so doing, we are mindful to connect our QFFM to the conventional Poiseuille and Ergun flow models, albeit through a modified version for terms, which corrects for the glaring shortcomings of each.

2.2. Fundamentals of the Q Fluid Flow Model (QFFM)

2.2.1. Particle

Let us define an obstacle to be placed within a packed conduit as a spheroidal particle of nominal diameter d_{pm} and sphericity Ω_p . Then we may write:

$$d_p = d_{pm} \Omega_p \quad (1)$$

Where, d_p =the spherical particle diameter equivalent $\Omega_p \leq 1$; thus, when $\Omega_p=1$, the particle is spherical.

Let the particle have a specific pore volume of S_{pv} , a skeletal density of ρ_{sk} , and a mass of m_p .

Let us define other particle characteristics as:

$$SA_p = \pi d_p^2 \quad (2)$$

And

$$CSA_p = \frac{\pi d_p^3}{4} \quad (3)$$

Where, SA_p =particle equivalent surface area; and CSA_p =particle equivalent cross sectional area.

It follows that we may write:

$$V_{dp} = \frac{\pi d_p^3}{6} \quad (4)$$

$$\rho_{part} = \frac{m_p}{V_{dp}} \quad (5)$$

Where, V_{dp} =the volume of a single spherical particle equivalent; ρ_{part} =the apparent particle density.

Let us define particle porosity as the ratio of free space within the particle to the total free space occupied by the particle as a whole, thus:

$$\varepsilon_p = S_{pv} \rho_{part} \quad (6)$$

Where, ε_p =the particle porosity.

It follows that:

When, $\varepsilon_p=1$, the particle is devoid of solid matter, i.e. contains only free space;

When, $\varepsilon_p=0$, the particle is made entirely of solid matter, i.e. the particle is non-porous;

When, $0 \leq \varepsilon_p < 1$, the particle is partially porous, i.e., consists of a solid particle skeleton plus internal pores.

2.2.2. Conduit

Let us define a fluid conduit as a right circular cylinder of length L and diameter D . Then we may write:

$$V_{ec} = \frac{\pi D^2 L}{4} \quad (7)$$

Where, V_{ec} = the volume of free space within an empty conduit.

Let the conduit be packed with n_p number of particle equivalents of diameter d_p .

It follows that we may write:

$$V_{part} = \frac{n_p \pi d_p^3}{6} \quad (8)$$

Where, V_{part} =the cumulative volume occupied by all the particle equivalents within a packed conduit.

Let us define as n_{pq} , the number of particle equivalents whose collective volume is equal to the volume of free space within an empty conduit.

It follows that we may write:

$$n_{pq} = \frac{V_{ec}}{V_{dp}} = \frac{3D^2 L}{2d_p^3} \quad (9)$$

Let us define the packed conduit fluidic architecture as:

$$\gamma = \frac{n_{pq} D}{L} \quad (10)$$

Where, γ =the fluidic architectural coefficient for a given packed conduit.

We now turn to conduit porosities.

Let us define the volume of free space within the packed conduit which is *external* to all the particles as V_e ; the volume of free space which is *internal* to all the particles as V_i ; the volume which is occupied by all the particle skeletons as V_{sk} ; and V_t as the *total* volume of free space within the packed conduit which is devoid of solid matter.

It follows that we may write:

$$(1 - \varepsilon_0) = \frac{n_p}{n_{pq}} = \frac{V_{part}}{V_{ec}} \quad (11)$$

Where, the conduit particle fraction, $(1-\varepsilon_0)$ =the volume fraction of the packed conduit occupied by the particles.

$$\varepsilon_{sk} = \frac{(1-\varepsilon_p)n_p}{n_{pq}} = \frac{V_{sk}}{V_{ec}} \quad (12)$$

Where, the conduit skeletal porosity, ε_{sk} =the volume fraction of the packed conduit occupied by the particle skeletons.

$$\varepsilon_0 = \frac{1-n_p}{n_{pq}} = \frac{V_e}{V_{ec}} \quad (13)$$

Where, the conduit external porosity, ε_0 =the volume fraction of the packed conduit *external* to the particles.

$$\varepsilon_i = \varepsilon_p (1 - \varepsilon_0) = \frac{V_i}{V_{ec}} \quad (14)$$

Where, the conduit internal porosity, ε_i =the volume fraction of the packed conduit *internal* to the particles.

$$\varepsilon_t = 1 - \frac{(1-\varepsilon_p)n_p}{n_{pq}} = \varepsilon_i + \varepsilon_0 \quad (15)$$

Where, the conduit total porosity, ε_t =the sum of the volume fractions *external* and *internal* to the particles.

It follows that *particle* porosity and *conduit internal* porosity are related as follows:

when $\varepsilon_p=0$, conduit internal porosity $\varepsilon_i=0$ and, thus, the particles are completely solid throughout, i.e., non-porous.

when $\varepsilon_p=1$, conduit internal porosity $\varepsilon_i=(1-\varepsilon_0)$ and thus, the particles are completely devoid of solid matter, i.e., totally porous.

Additionally, it follows that reconciling the definitions above for solid matter and lack thereof, i.e., porosity, within a conduit, [see Eqs. (8) and (11) above], we may now write:

$$\frac{n_p \pi d_p^3}{6} = V_{ec} abs(1 - \varepsilon_0) \quad (16)$$

Equation (16) reconciles the distribution of free space within the conduit according to the conservation Laws of Nature, whereby all partial volume fractions of the fluid-filled packed conduit, whether occupied by solid matter or fluid, add to unity.

2.2.3. The Conservation Laws Governing Packed Conduits

Thus, the Conservation Laws pertaining to packed conduits dictate that we may write:

$$\varepsilon_0 + \varepsilon_i + \varepsilon_{sk}=1 \quad (17)$$

or

$$\varepsilon_t + \varepsilon_{sk}=1 \quad (18)$$

Let us define the packing density of a packed conduit as:

$$\rho_{pack} = \frac{M_p}{V_{ec}} \quad (19)$$

Where, ρ_{pack} =the packing density of the packed conduit; $M_p=n_p m_p$, the total mass of all the particles in a packed conduit under study.

It follows that we may now write:

$$\varepsilon_0=1-\rho_{pack}(S_{pv}-1/\rho_{sk}) \quad (20)$$

or

$$\varepsilon_0=1- [2n_p d_p^3/(3D^2L)] \quad (21)$$

Accordingly, we may write:

$$\varepsilon_p = \frac{\varepsilon_t - \varepsilon_0}{1 - \varepsilon_0} \quad (22)$$

Substituting for the independently measured components of ε_p in Equation (22), gives

$$S_{pv} \rho_{part} = \frac{\varepsilon_t - \varepsilon_0}{1 - \varepsilon_0} \quad (23)$$

It therefore follows that, empirically, we may define a packed conduit in terms of 4 *independent* variables (M_p , V_{ec} , S_{pv} , ρ_{sk}) or, alternatively, (n_p , d_p , D , L), *in combination with* one *dependent* variable (ε_0), all of which are *measurable*. However, if in addition to measuring the independent variables, one also measures the value of the external porosity, ε_0 (a dependent variable), both sides of Equations (22) and (23) must be reconciled for any given packed conduit under study, *as dictated by the Conservation Laws*

(sometimes referred to as the Laws of Continuity when their application involves moving entities like the fluid in this particular application). This dictate from the Laws of Continuity *trumps all measurement techniques*, which generally lack the specificity/accuracy to balance either equation without the need for further reconciliation or modification.

Thus, the left hand side of Equation (23) contains measurements made *outside* of the packed conduit, i.e., independent of the packed conduit under study, whereas the right hand side of Equation (23) contains measurements made *within* the packed conduit under study. Accordingly, balancing of Equation (23) is always necessary to validate the accuracy of the reported values for the measured parameters of the packed conduit under study.

It follows that, in the case of packed conduits which contain nonporous particles, Equation (23) is equal to zero on both sides of the equalization sign, thus eliminating the need to reconcile column porosity and particle porosity.

2.2.4. The Q-Porosity Function (ε)

Let us now collect all the partial porosity definitions in the QFFM underlying packed conduits which are defined in terms of particle size equivalents and view them as dimensionless mathematical functions of n_p , which we will designate as Q-Porosity functions. There are a total of 5 such functions, which we view in the context of the generalized Q-Porosity function ε .

1. $(1-\varepsilon_0)=n_p/n_{pq}$, Equation (11) above.
2. $\varepsilon_{sk}=(1-\varepsilon_p)n_p/n_{pq}$, Equation (12) above.
3. $\varepsilon_0=(1-n_p/n_{pq})$, Equation (13) above.
4. $\varepsilon_i=\varepsilon_p (n_p/n_{pq})$, Equation (14) above.
5. $\varepsilon_t=1- (1-\varepsilon_p)n_p/n_{pq}$, Equation (15) above.

It now becomes obvious that the Q-Porosity functions ε_0 and $(1-\varepsilon_0)$ are *independent* of the value of the particle porosity, ε_p .

Similarly, it is also obvious that the Q-Porosity functions ε_i , ε_{sk} and ε_t are *dependent* on the value of the particle porosity, ε_p .

2.3. The Conduit Packing Process

2.3.1. Solid Particles ($0 \leq \varepsilon_p < 1$)

Let us now define the conduit packing process in the case of solid particles ($0 \leq \varepsilon_p < 1$) by viewing the role of our independent variable, n_p , within the context of the Q-Porosity function (ε). This is best accomplished by viewing a worked example on a plot of the dimensionless Q- Porosity function, ε , versus the number of particle equivalents, n_p .

Our chosen worked example consists of 10 micron particles packed into a conduit of dimensions 10 cm in length and 0.46 cm in diameter, the details for which are presented in Figure 1, for the case in which the particles are nonporous ($\varepsilon_p=0$).

As shown in Figure 1 below, our empirical packing process recognizes Kepler's conjecture regarding the stacking of solid spheres. Accordingly, the maximum value of the Q-Porosity function $(1-\varepsilon_0)$ is approximately 0.74 with

the corresponding minimum value of approximately 0.26 for the Q-Porosity function ϵ_0 . Kepler's conjecture is a consequence of the fact that solid spheres and free space are *mutually exclusive* and therefore the maximum value of n_p achieved empirically must be less than the value of n_{pq} . The upper limit of the value of n_p is always n_{pq} since it represents

the most particle equivalents, *theoretically*, that could be packed into any given conduit under study.

Accordingly, the theoretical *domain* of the Q-Porosity function (ϵ) runs from 0 to n_{pq} and the *ranges* of the function vary between the values of 0 and 1, as shown in Figure 1.

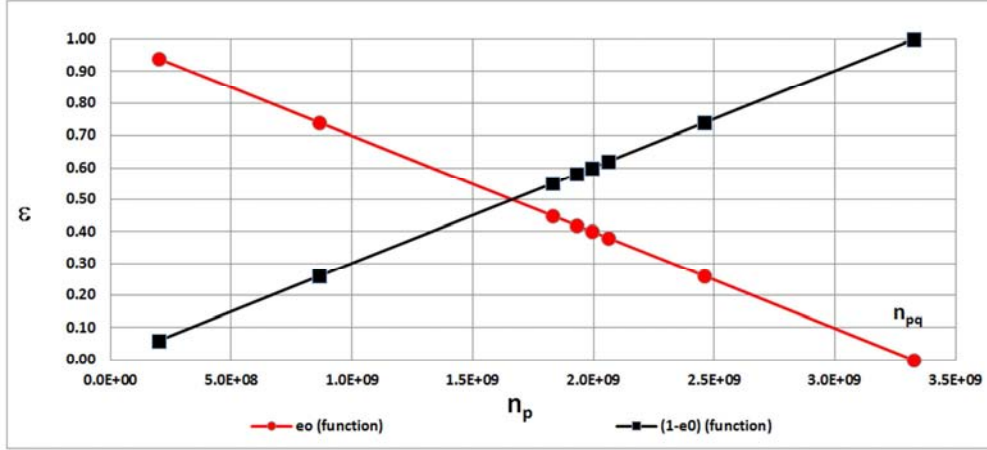


Figure 1. Q-Porosity Function for Non-Porous Particles ($\epsilon_p=0$).

In Figure 1 we only display two of the Q-Porosity functions, i.e., ϵ_0 and $(1-\epsilon_0)$, since they are not influenced by the particle porosity value, ϵ_p , and, in this particular case ($\epsilon_p=0$), $\epsilon_i=0$, $\epsilon_t=\epsilon_0$ and $\epsilon_{sk}=(1-\epsilon_0)$. Additionally, we note that these two functions are *reciprocal* in nature to the extent that as one increases, the other decreases, all as a function of n_p .

We now further refine the definition of the entity n_p to be that of a *vector* rather than a *scalar* quantity and, therefore, *confer upon it a directional component* in addition to its mandatory *magnitude* component.

Let us now define the *packing process of a conduit*, using our example with solid particles, in terms of our mathematical Q-Porosity functions, as the direction of increasing *positive* values of n_p . Thus, as we move along the x axis of Figure 1 in the direction of left to right, starting at the origin of the plot at $n_p=0$, the corresponding values on the y axis represent the changing characteristics of the Q-Porosity function ϵ in the filling (packing) process. At the

starting point of $n_p=0$, the conduit is devoid of particles (contains only free space) and at the maximum value of n_p achieved in the filling process, the conduit is fully packed. Accordingly, filling of a “packed” conduit with solid particles is represented by the increasing positive values of n_p , i.e., the motion left to right along the x axis of the plot starting at the value of $n_p=0 \rightarrow$.

We shall now consider the more complex packing process in which the particle porosity varies between the values of 0 and 1, i.e., the case of partially porous particles ($0 < \epsilon_p < 1$). In our worked example shown in Figure 2, we show as our example a packed conduit with particles which have a particle porosity of 0.6 ($\epsilon_p=0.6$). Because the porosity functions of ϵ_i , ϵ_t and ϵ_{sk} are dependent on the value of ϵ_p , we include these functions in our Figure 2.

As displayed in Figure 2, each of the 5 porosity functions, ϵ_0 , $(1-\epsilon_0)$, ϵ_i , ϵ_t , and ϵ_{sk} have discrete and different values for all values of n_p .

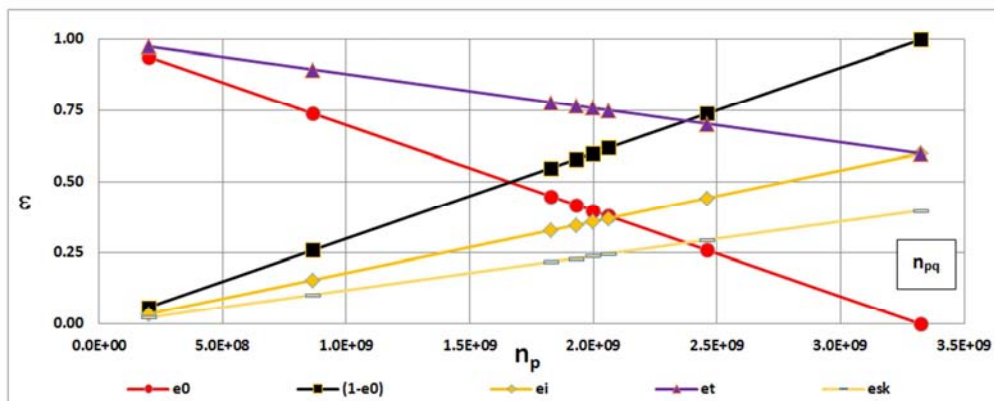


Figure 2. Q-Porosity Function for Partially Porous Particles ($0 < \epsilon_p < 1$).

2.3.2. Hypothetical Q-Particles ($\epsilon_p=1$)

We shall now consider the packing process in the *special case* when the particles are *fully* porous, i.e., they are completely made of free space ($\epsilon_p=1$). This scenario is presented in Figure 3.

As shown in Figure 3, our packing process for particles

made of free space ($\epsilon_p=1$), which we designate as hypothetical Q-particles, is represented by increasingly *negative* values of n_p . Accordingly, the domain of the Q-Porosity function runs from 0 to $-n_{pq}$. Similarly, it follows that the range of the function varies between the values of -1 and 2, as shown in the plot.

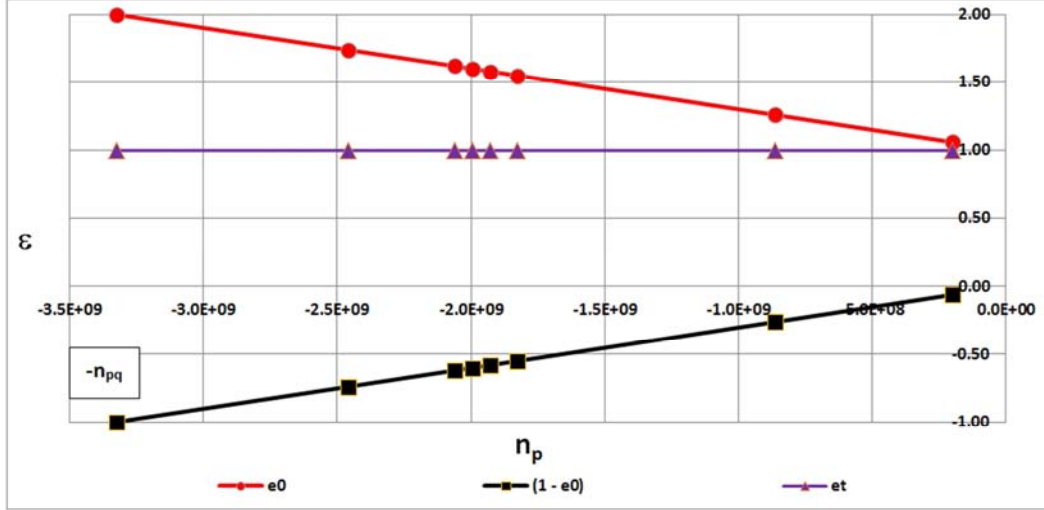


Figure 3. Q-Porosity Function for Fully Porous Particles ($\epsilon_p=1$).

In this scenario the Q-Porosity functions $\epsilon_t=1$ and $\epsilon_{sk}=0$ for all values of n_p . The function ϵ_i has identical values to the function $(1-\epsilon_0)$ and varies between 0 and -1, whereas the value of the function ϵ_0 varies between 1 and 2.

Let us now define the directional component of packing a conduit with hypothetical Q-particles in terms of our mathematical Q-Porosity functions. As we move along the x axis of Figure 3 in the direction of right to left, starting at the origin of the plot at $n_p=0$, the corresponding values on the y axis represent the changing characteristics of the Q-Porosity function ϵ in the filling (packing) process. This direction of filling is the opposite of that for solid particles. At the starting point of $n_p=0$, we consider the conduit to be devoid of all particles (including particles of free space) and at the maximum value of $n_p=-n_{pq}$ achieved in the filling process, the conduit is fully packed with particles of free space

(hypothetical Q-particles). Accordingly, filling of a “packed” conduit with hypothetical Q-particles is represented by increasing negative values of n_p , i.e., the motion right to left along the x axis of the plot starting at $n_p=0 \leftarrow$.

It follows that in the case of hypothetical Q-particles which are made of free space, Kepler's conjecture does not apply, since particles of free space are *mutually inclusive* with free space, i.e., they *are* free space. Accordingly, the maximum value of n_p achieved empirically is $-n_{pq}$, which corresponds to the conduit being filled with free space, and is also the upper *theoretical* limit of n_p in these circumstances.

We choose to use, advantageously, the *absolute value* of the porosity function $(1-\epsilon_0)$ in our theoretical development, which represents the *magnitude* of the function and is, therefore, always positive, as shown in Figure 4.

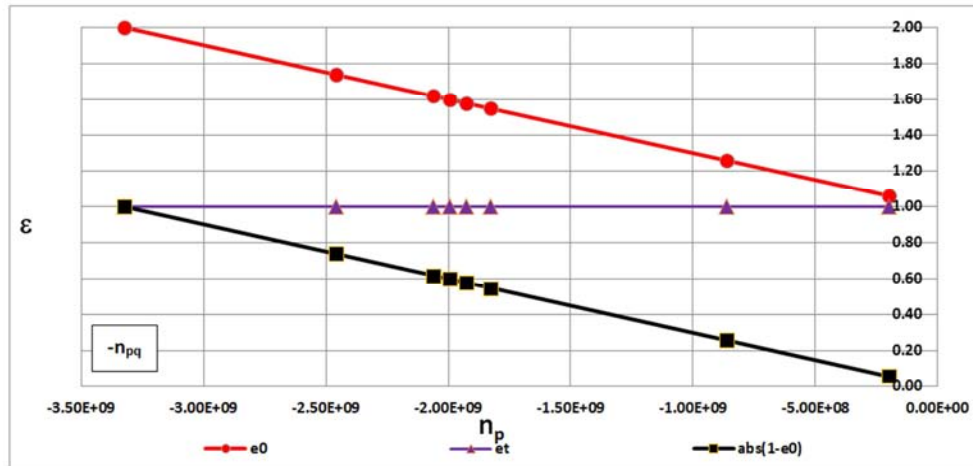


Figure 4. Q-Porosity Function for Fully Porous Particles ($\epsilon_p=1$).

Accordingly, as shown in Figure 4, the *ranges* of all Q-Porosity functions of interest in this special case have positive magnitudes, and vary between the values of 0 and 2.

2.3.3. The Packed Conduit Hypothetical Q Channel Defined

Let us define a hypothetical *cylindrical* fluid channel within a packed conduit, which we shall call the hypothetical Q channel (HQC), whose characteristic dimensions are defined as:

$$d_c = \frac{d_p}{\text{abs}(1-\varepsilon_0)} = \frac{d_p}{\text{abs}(n_p/n_{pq})} \quad (24)$$

Where, d_c =the diameter of the HQC.

It follows that we may write [see Eqs. (7) and (14)]:

$$V_c = V_{ec}\varepsilon_t = \frac{\pi n_{pq} d_p^3 \varepsilon_t}{6} \quad (25)$$

Where, v_c =the volume of the HQC.

It follows that we may also write:

$$a_c = \frac{\pi d_c^2}{4} = \frac{\pi n_{pq}^2 d_p^2}{4 n_p^2} \quad (26)$$

Where, a_c =the cross sectional area of the HQC.

Similarly, we may write:

$$\varepsilon_p=1; n_p=-n_{pq}; d_p=D=d_c; l_c=L; v_c=V_{ec}; \text{abs}(1-\varepsilon_0)=1; \varepsilon_0=2; \varepsilon_t=1; \delta=0.125 (1/8); \gamma=1.5 (3/2); \tau=0.188 (3/16).$$

To further articulate the characteristics of the Unit HQC in the case of our chosen worked example, we present here 4

Where, l_c =the length of the HQC.

Let us define the Unit Hypothetical Q Channel as a *special case* of the more general HQC. It is defined as a conduit filled with hypothetical Q-particles having two *fixed* boundary conditions: (1), $d_p=D$ and (2), $n_p=-n_{pq}$.

It follows that, since the function $\varepsilon_0=2$ when $n_p=-n_{pq}$, the function $\text{abs}(1-\varepsilon_0)=1=\varepsilon_t$.

Accordingly, any “empty” conduit/capillary is represented in the QFFM by what we now term the Unit HQC since, by definition, its Q-Porosity functions of $[\text{abs}(1-\varepsilon_0)]$ and ε_t are unity, as shown above in Figure 4 for our worked example.

As shown in Figure 5 below, any conduit/capillary when totally filled with hypothetical Q-particles ($n_p=-n_{pq}$), whose diameters are equivalent to the diameter of the conduit ($d_p=D=d_c$), will *always* have the *constant* values shown below, regardless of what the conduit dimensions are.

Thus, an empty conduit/capillary is defined in the QFFM as a packed conduit containing hypothetical particles with a particle porosity of unity ($\varepsilon_p=1$), and is represented by the Unit HQC with the following *constant* values:

graphical representations of the primary channel functions; see Figures 5, 6, 7 and 8.

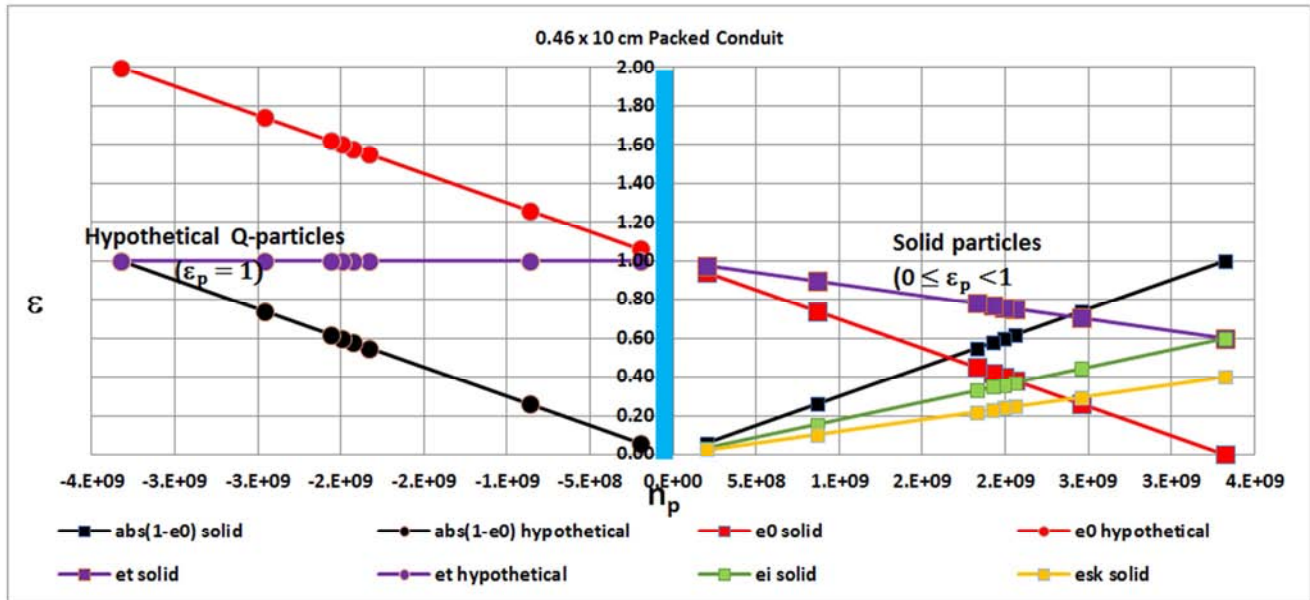
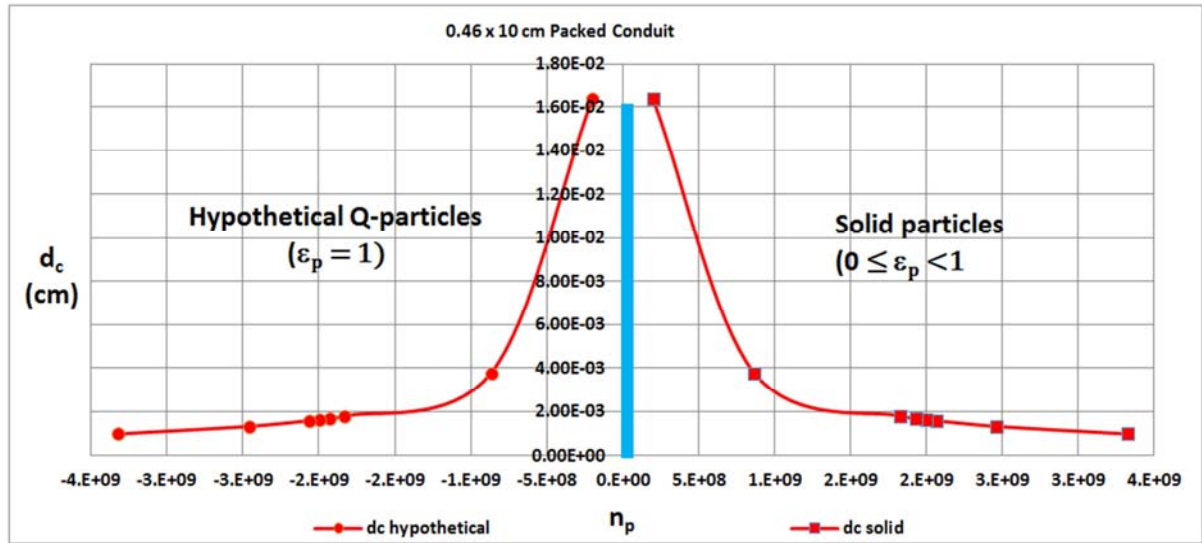
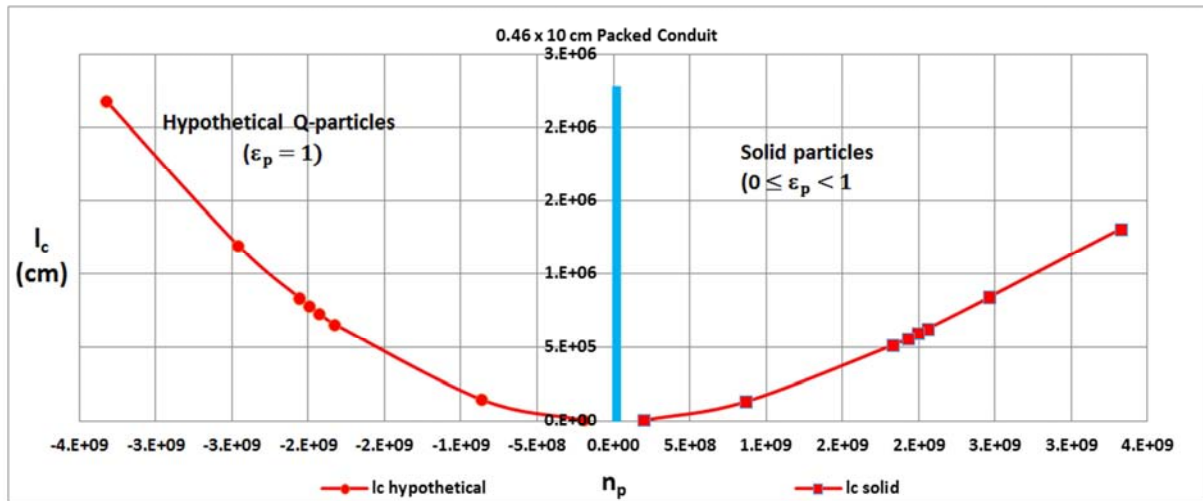
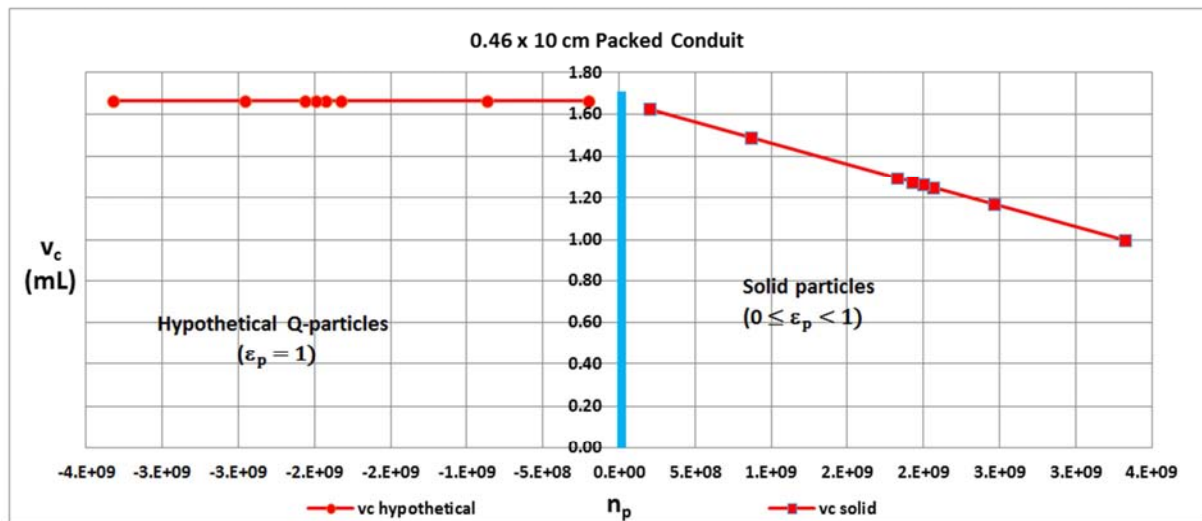


Figure 5. The HQC (Q-Porosity Function).

Figure 6. The HQC (d_c function).Figure 7. The HQC (l_c function).Figure 8. The HQC (v_c function).

As shown in Figure 5, the vertical line in the range of the Q-Porosity function (ϵ), i.e., $n_p=0$, represents the axis of

symmetry between the half-plane Q-Porosity function for solid particles, on the one hand (right hand side half-plane), and hypothetical Q particles, on the other hand (left hand side half-plane). Note that the Q-Porosity functions are *discontinuous* at the value of $n_p=0$, but are *continuous* at all other values of n_p , i.e., $-n_{pq} \leq n_p < 0$; $0 < n_p \leq n_{pq}$.

It follows that, as shown in Figure 6, the HQC function d_c is correspondingly discontinuous at the value of $n_p=0$, since at this precise value the *diameter* of the HQC tends to infinity. Thus, in the QFFM, the “infinite diameter packed conduit” is prohibited by hypothesis.

Finally, it follows that, as shown in Figure 7, the HQC

2.4. Fluid Motion in the HQC

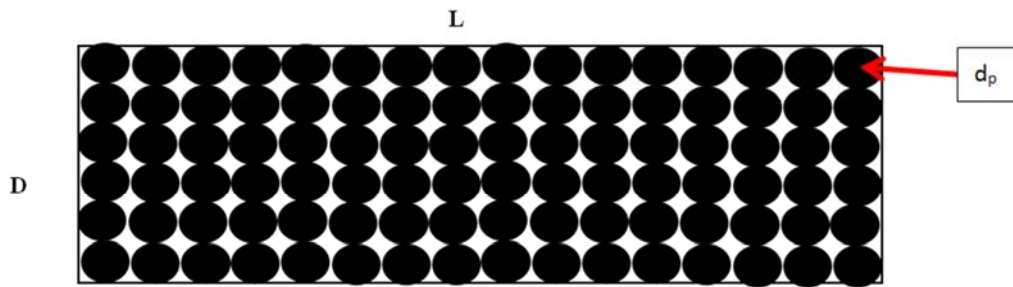


Figure 9. Physical Reality underlying the HQC.

Let us consider the motion of the fluid in the HQC as a *control volume element* of fluid flowing through a packed conduit under study with a volumetric flow rate, q ; fluid absolute viscosity η ; fluid density ρ_f , and under a differential pressure, ΔP , defined as:

$$\Delta P = P_1 - P_0 \quad (28)$$

Where, ΔP =the differential pressure drop across the packed conduit; P_1 =hydraulic pressure at conduit inlet; P_0 =hydraulic pressure at conduit outlet [See Figure 9].

We shall now develop the interrelationships among the conduit parameters which characterize the motion of the fluid within the HQC. In so doing, we derive a unique relationship between the driving force for fluid flow, which is known generally as the pressure gradient, and other HQC variables.

Let Q be the position at any time t of a point describing a circle of radius a with uniform angular velocity ω about the center O . Let P be the projection of Q on any diameter $A'O A$. Let the angle $AOQ = \Phi$. And let $OP = x$ [See Figure 10].

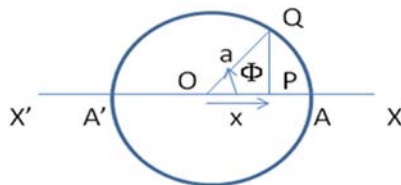


Figure 10. Uniform Circular Motion.

Thus:

$$\frac{d(\Phi)}{dt} = \omega \quad (29)$$

function l_c is zero at the value of $n_p=0$. In addition, the value of l_c is always greater for values of n_p less than zero, than for values of n_p greater than zero, a consequence of a value for external porosity in excess of unity, in this half-plane of the function.

Similarly, it follows that, as shown in Figure 8, the HQC function v_c is correspondingly discontinuous at the value of $n_p=0$, since at this precise value, the volume of the HQC is *undefined*, but at all values of n_p less than zero, its volume is a *constant* positive value and at all values of n_p greater than zero, it has a *variable* positive value.

where ω is a constant

Hence,

$$\Phi = (\omega t + \alpha) \quad (30)$$

where ω and α are constants

Hence,

$$x = a \cos \Phi = a \cos (\omega t + \alpha) \quad (31)$$

In Eq. (32) below, we shall define the meaning of each of the flow terms in Eq. (30) as they relate to the parameters of the packed conduit embodied in the concept of the HQC.

We begin with the hypothesis that the motion of the fluid within the HQC is defined by that of uniform circular motion and, accordingly, the general equation of Simple Harmonic Motion (SHM), represented by Equation (30);

Where, Φ =the phase of the motion; ω =the frequency of the motion; t =the elapsed time of the motion; α =the epoch of the motion, all as taught in the general theory of classical mechanics [25].

Let $\Phi = P_Q$; $\omega = \lambda / \phi_h$; $t = Q_N$; $\alpha = 2\pi k_1 / 360$; and $q = dV/dt$.

Where, P_Q =instantaneous HQC drag normalized viscous friction factor; ω =instantaneous HQC fluid resistance; λ =instantaneous HQC wall-adjusted fluid current normalization coefficient; ϕ_h =drag normalized hydraulic channel circumference; Q_N =instantaneous fluid current; k_1 =the drag normalized wetted surface area; and V =a control volume of fluid.

For clarity here, in our modeling of the fluid motion in the HQC, we recite our procedure of equating normalized

dimensionless parameters related to the HQC to *dimensional* parameters in our SHM model. Thus, for instance, the dimensionless parameter Q_N of the HQC is equated to the elapsed time parameter t , of the SHM model, which has the dimensional units of seconds.

Note also that we have *arbitrarily* chosen the units of *radians* in our definition of the epoch of the motion in the SHM model, by virtue of the unit conversion ($2\pi/360$), which is the conversion factor between degrees and radians.

Thus, substituting for the terms which define our fluid motion in the HQC, we may now rewrite Equation (30) as follows:

$$P_Q = (k_1 + \lambda Q_N / \phi_h) \quad (32)$$

It follows that we may state that, in the limit as Q_N tends to zero, the value of P_Q approaches the constant value of k_1 . We can express this algebraically as:

$$\begin{aligned} P_Q &= k_1 \\ \text{Lim}_{Q_N \rightarrow 0} \end{aligned}$$

Thus, the function P_Q is bounded only on one side and varies from a minimum value of k_1 on the low side, when the fluid is at rest ($Q_N=0$), and is unbounded on the high side (high value of Q_N).

Let us define a corresponding HQC kinetic friction factor as:

$$P_K = \frac{P_Q}{Q_N} \quad (33)$$

Where, P_K =the instantaneous HQC normalized kinetic

friction factor.

Thus, the function P_K is *infinite* when the fluid is at rest ($Q_N=0$).

Driven by the principle of avoiding *non-finite* boundaries, let us define the reciprocal of Equation (33) as:

$$\frac{1}{P_K} = \frac{Q_N}{P_Q} = \Theta \quad (34)$$

Where, Θ =the dimensionless permeability of the HQC.

It follows that we may write:

$$\Theta = \frac{1}{k_1/Q_N + \lambda/\phi_h} \quad (35)$$

It further follows that we may now state that, in the limit, as the value of Q_N tends to infinity:

$$\begin{aligned} \Theta &= \phi_h \\ \text{Lim}_{Q_N \rightarrow \infty} \end{aligned}$$

Similarly, we may state that, in the limit, as Q_N tends to zero:

$$\begin{aligned} \Theta &= 0 \\ \text{Lim}_{Q_N \rightarrow 0} \end{aligned}$$

Thus, the dimensionless permeability function of the HQC, Θ , is *finite* on both sides and varies between the minimum limit of 0 on the low side and the maximum limit of ϕ_h/λ , on the high side.

The dimensionless parameters of the HQC are shown in Figure 11 below, in a log-log plot against Q_N .

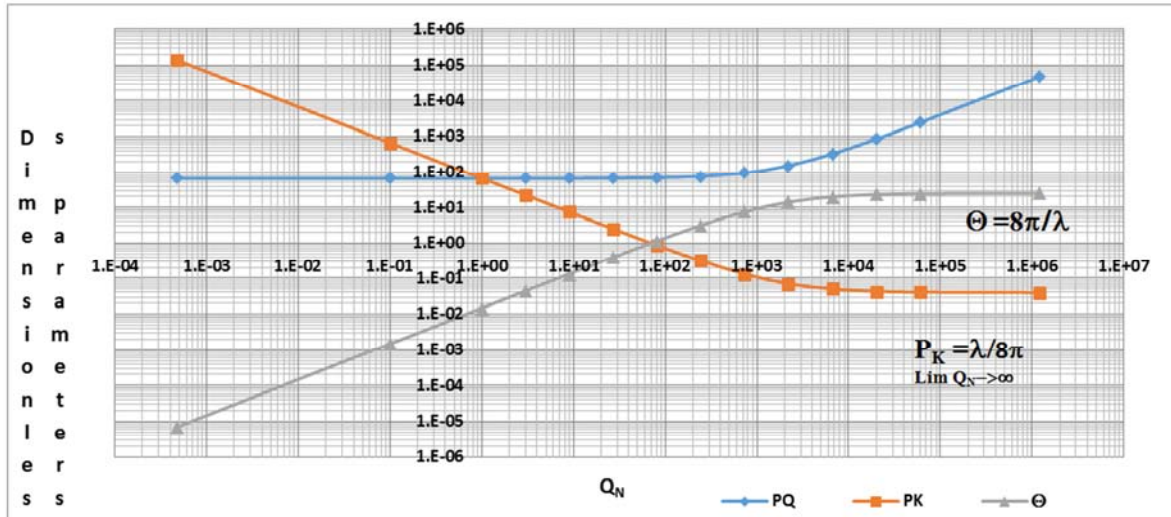


Figure 11. HQC-Dimensionless Parameters.

Let us now define k_2 , the drag normalized hydraulic and channel perimeter, a normalization coefficient, as:

$$k_2 = \frac{1}{2\pi r_h} \quad (36)$$

and

$$\phi_h = 2\pi r_h \quad (37)$$

$$r_h = \frac{SA_p}{CSA_p} = 4 \quad (38)$$

Where, k_2 =fluid motion dynamic constant; r_h =the normalization coefficient of fluid drag.

Let us now define k_1 , the drag normalized wetted surface

area, a normalization coefficient, as:

$$k_1 = \frac{4\pi r_h^2}{3} = \frac{64\pi}{3} \quad (39)$$

It follows that we may now rewrite Equation (32) as:

$$P_Q = \frac{64\pi}{3} = \frac{\lambda Q_N}{8\pi} \quad (40)$$

Let us define δ , a porosity normalization coefficient, as:

$$\delta = \frac{1}{\varepsilon_0^3} \quad (41)$$

Let us define τ , a tortuosity normalization coefficient, as:

$$\tau = \delta\gamma \quad (42)$$

Let us now define Q_N , the instantaneous fluid current, a dimensionless parameter, as:

$$Q_N = \delta R_{em} \quad (43)$$

Where, R_{em} = the modified Reynolds number, defined below in Eqs. (54), (55) and (57).

Let us now define λ , the HQC wall-adjusted fluid current normalization coefficient, as:

$$\lambda = (1 + W_N) \quad (44)$$

Where, W_N = the net wall effect, and is restricted to where $0 \leq W_N$

It follows that we may now rewrite Equation (40) as:

$$P_Q = \frac{64\pi}{3} = \frac{\delta \lambda R_{em}}{2\pi r_h} \quad (45)$$

Substituting for λ in Equation (45), gives:

$$P_Q = \frac{64\pi}{3} = \frac{\delta(1+W_N)R_{em}}{2\pi r_h} \quad (46)$$

Let us further refine the definition of W_N as:

$$W_N = W_1 + W_{2R} \quad (47)$$

Where, W_1 = the primary wall effect, defined below; W_{2R} = the residual secondary wall effect, defined below.

Let us define ω_0 , the dimensionless resistance of the fluid in the absence of any wall effect ($\lambda=1$), i.e., $W_N=0$, as follows:

$$\omega_0 = \frac{1}{\phi_h} \quad (48)$$

Let us define β_0 , the dimensionless fluid/wall boundary layer in the absence of wall effect ($\lambda=1$), i.e., $W_N=0$, as follows:

$$\beta_0 = \frac{k_1}{\omega_0 Q_N + k_1} = \frac{k_1}{Q_N / \phi_h + k_1} \quad (49)$$

Let us define W_1 , the dimensionless boundary layer component of fluid current, which we will refer to as the *primary* wall effect, as follows:

$$W_1 = \frac{\beta_0^{1/3}}{\tau} \quad (50)$$

Let us define k_{dc} , the channel relative wall surface roughness coefficient, as follows:

$$k_{dc} = \frac{k}{d_c} \quad (51)$$

where, k is a measure of wall roughness.

Let us define W_2 , the wall roughness component of fluid current, which we will refer to as the *secondary* wall effect, as follows:

$$W_2 = 30k_{dc}^{(1/3)} \quad (52)$$

Note that the value of 30 appearing in Equation (52) is not based upon any fundamentally derived concept but rather on our empirical data. We are confident, however, that this value has to do with end-effects of the packed conduit but have not as of this writing been able to define it in more precise terms.

Let us define W_{2R} , the residual wall roughness component of fluid current, as follows:

$$W_{2R} = W_2 - W_1^{1.2} \quad (53)$$

We pause here, yet again, to explain the origin of the exponent of 1.2 appearing in Equation (53). Because we have based our definition of the boundary layer on a *theoretical asymptote*, i.e., $\lambda=1$, which is never *precisely* the case in real life, we have included this exponent value as a correction factor to account for this *assumption* in our theoretical model.

Let us define the modified Reynolds number as:

$$R_{em} = \frac{n_k}{n_v} \quad (54)$$

Where, n_k = the kinetic hydraulic force exerted per unit element of fluid control volume; n_v = the viscous hydraulic force exerted per unit element of fluid control volume.

Let n_k , the *kinetic* hydraulic force per unit element of fluid control volume, be defined as:

$$n_k = \frac{\delta \mu_s^2 \rho_f}{d_c} \quad (55)$$

Where, μ_s = fluid superficial velocity, which, in turn, is defined as:

$$\mu_s = \frac{4q}{\pi D^2} \quad (56)$$

In a dimensional analysis using the cgs convention, we demonstrate the dimensional integrity of n_k , thusly;

$$\begin{aligned} n_k &= (\text{cm}^3 \text{sec}^{-1})^2 (\text{gcm}^{-3}) (\text{cm}^{-4} \text{cm}^{-1}) \\ &= \text{gcm}^{-2} \text{sec}^{-2} \\ &= \text{Force/Volume} \end{aligned}$$

Let n_v , the *viscous* hydraulic force per unit element of fluid control volume, be defined as:

$$n_v = \frac{\delta \mu_s \eta}{d_c^2} \quad (57)$$

Similarly, in a dimensional analysis using the cgs convention, we demonstrate the dimensional integrity of n_v , thusly:

$$\begin{aligned} n_v &= (\text{cm}^3 \text{sec}^{-1})^2 (\text{gcm}^{-3} \text{sec}^{-1}) (\text{cm}^{-2} \text{cm}^{-2}) \\ &= \text{gcm}^{-2} \text{sec}^{-2} \\ &= \text{Force/Volume} \end{aligned}$$

Finally, let us define BLT, the fluid wall boundary layer thickness, as follows:

$$\text{BLT} = \frac{\beta d_c}{2\tau} \quad (58)$$

2.5. Quinn's Law

We may now restate equation (40) as:

$$P_Q = \frac{4\pi r_h^2}{3} + \frac{\delta \lambda n_k}{2\pi r_h n_v} \quad (59)$$

Let us define the dimensionless *drag* normalized pressure gradient as:

$$\frac{\Delta P}{r_h n_v L} = P_Q \quad (60)$$

Where, $\Delta P/L$ =the pressure gradient; $\Delta P/(r_h L)$ =*drag* normalized pressure gradient.

$\Delta P/(r_h n_v L)$ =*drag* normalized viscous friction factor.

Then, substituting for P_Q in Equation (59), we may write:

$$\frac{\Delta P}{r_h n_v L} = \frac{4\pi r_h^2}{3} + \frac{\delta \lambda n_k}{2\pi r_h n_v} \quad (61)$$

Multiplying across by n_v in Equation (61) gives:

$$\frac{\Delta P}{r_h L} = \frac{4\pi r_h^2 n_v}{3} + \frac{\delta \lambda n_k}{2\pi r_h} \quad (62)$$

We can describe Equation (62) as: *drag* normalized pressure gradient=(viscous term) + (kinetic term)

Equation (62) represents the *instantaneous balanced* equation with respect to the distribution of forces between the contributions of *viscous* and *kinetic* considerations. Unfortunately, however, it is not a useful equation from an *empirical* perspective, because *in practice* we measure ΔP , not $(\Delta P/r_h)$.

Accordingly, multiplying across by r_h in Equation (62), gives:

$$\frac{\Delta P}{L} = \frac{4\pi r_h^3 n_v}{3} + \frac{\delta \lambda n_k}{2\pi} \quad (63)$$

Substituting for n_v [Eq. (57)] and n_k [Eq. (55)] in Equation (63), gives:

$$\frac{\Delta P}{L} = \frac{4\pi r_h^3 \delta \mu_s \eta}{3 d_c^2} + \frac{\delta^2 \lambda \mu_s^2 \rho_f}{d_c} \quad (64)$$

Therefore, empirically, Equation (64) is the most useful equation for any practitioner. It demonstrates that when the fluid velocity, μ_s , tends to zero, (fluid at rest), and, therefore, the kinetic term (2nd term on right hand side of Equation (64)) is

negligible, the *control volume element coefficient* is represented by $4\pi r_h^3/3=256\pi/3=268$ approx., since this is the multiplier in the viscous term of Equation (64) corresponding to the pressure gradient $\Delta P/L$. In other words, the *entire* control volume element is assigned to *viscous* considerations only, and is represented by the volume of a sphere having a radius r_h , the coefficient of fluid drag. We can show this algebraically, as follows (neglecting the kinetic term in Equation (63)):

$$\frac{\Delta P}{L} = \frac{4\pi r_h^3 n_v}{3} \quad (65)$$

Equation (65) represents the empirically meaningful relationship between the *measured* pressure gradient (left hand side), and the fluid motion term (right hand side) when the fluid flow rate is very close to zero, i.e., kinetic contributions are negligible. Note that in this fluid flow regime, the fluid motion term is the product of two entities: n_v =the viscous hydraulic force exerted per unit element of fluid control volume and $(4\pi r_h^3/3=268)$ a/k/a the “viscous constant”.

[Incidentally, we point out that the value of 270 for the viscous constant in the Kozeny/Blake equation was identified as early as 1965 by J. C. Giddings [26, 27].]

We can now appreciate that the distribution of forces between viscous and kinetic contributions is captured by maintaining the *drag-normalized* value of the *viscous* fluid control element normalization coefficient, $k_1=64\pi/3$ and the *drag-normalized* value of the *kinetic* fluid control element normalization coefficient, $k_2=1/(8\pi)$. Thus, the constant k_1 acts as a dimensionless normalization coefficient for the hydraulic *viscous* forces, on the one hand, and k_2 acts as a dimensionless normalization coefficient for the hydraulic *kinetic* forces, on the other hand. In addition, note that in the viscous term, this normalization coefficient is *directly* proportional to the *second power* of the drag coefficient, whereas in the kinetic term, it is *inversely* proportional to the *first power* of the drag coefficient, which is exactly what we intuitively observe in the world around us. In other words, our experience tells us that as the surface area in contact with the flowing fluid increases, the pressure gradient increases (direct proportionality); but as the diameter of a conduit increases, the pressure gradient decreases (indirect proportionality).

We digress at this point to mention an aspect of our theoretical model which contradicts a common feature of conventional wisdom. That feature is the notion that the Reynolds number, R_e , is the ratio of kinetic to viscous forces. Correctly stated, the modified Reynolds number, R_{em} , is the ratio of the kinetic forces *per unit control volume element* to the viscous forces *per unit control volume element*, which involves the ratio of k_1/k_2 , a discrepancy factor of approximately 1,686.

The conventional Reynolds number concept, R_e , was derived by Sir Osborne Reynolds (1883) in experiments based upon an “idealized” fluid flow channel, the wall roughness and boundary layer of which he did not take into account. *His* idealized channel, therefore, would be represented by values for $\delta=1$ and $\lambda=1$, in *our* model, i.e., no wall effect of any kind and an *undefined* kinetic component of driving force, ΔP , since the value of $\delta=1$ represents a point

of discontinuity in the Q porosity function, ε . Accordingly, one could argue that the concept of the conventional Reynolds number is an *undefined* parameter in the real world, which might explain many of the anomalies in conventional wisdom, not the least of which is the inability to provide an analytical solution to the Navier-Stokes equation.

Now that we have properly balanced the pressure flow equation and assigned the correct variables to each of its compartments with respect to the contributions of viscous and kinetic considerations, and, in addition, have quantified the pressure gradient by setting the correct *magnitude* of the control volume element of fluid, we may proceed to gather terms and evaluate the various physical phenomena occurring within the flowing fluid channel.

Let us now define the wall-adjusted fluid current as:

$$\lambda Q_n = C_Q \quad (66)$$

Where, C_Q =the dimensionless wall-adjusted fluid current. It follows that we may now write:

$$\beta = \frac{k_1}{\omega Q_N + k_1} \quad (67)$$

Where, β =the instantaneous fluid/wall boundary.

It also follows that we may now rewrite Equation (40) as:

$$P_Q = \frac{64\pi}{3} + \frac{C_Q}{8\pi} \quad (68)$$

We hereby designate Equation (68) as Quinn's Law of Fluid Dynamics. It states that all pressure-driven flow in closed conduits can be represented by a *linear* dimensionless relationship, having a constant slope of $1/(8\pi)$ and an intercept of $64\pi/3$. This relationship is shown in Figure 12.

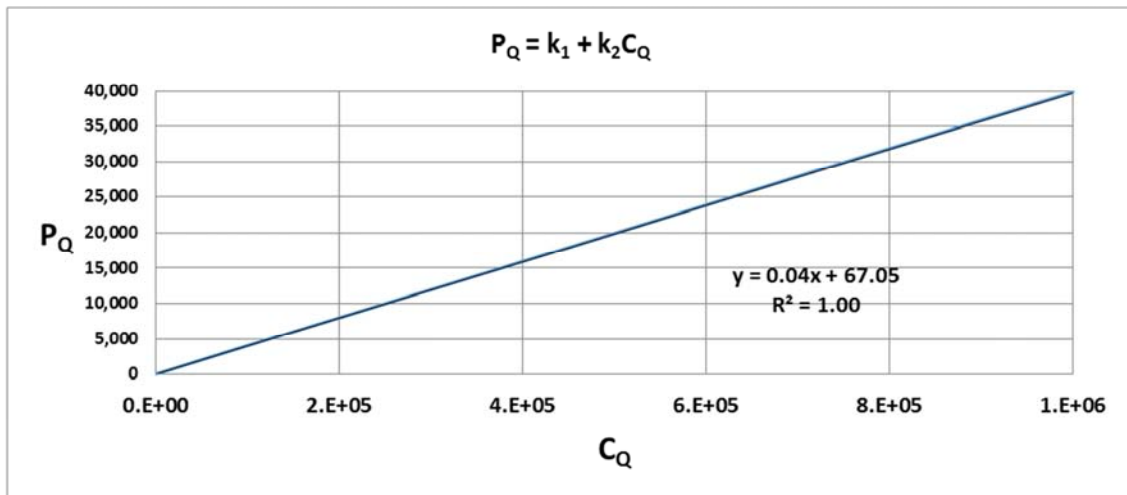


Figure 12. Quinn's Law of Fluid Dynamics.

If we replace the velocity term in Equation (64) by a flow rate term and substitute $r_h=4$, we get:

$$\frac{\Delta P}{L} = \frac{1024\delta q\eta}{3D^2 d_c^2} + \frac{8\delta^2 \lambda q^2 \rho_f}{\pi^3 D^4 d_c^5} \quad (69)$$

In the special case of an empty conduit, where $\delta=1/8$, $d_c=D$ and $\pi=22/7$, it follows that we may write:

$$\frac{\Delta P}{L} = \frac{128q\eta}{3D^4} + \frac{\lambda q^2 \rho_f}{248D^5} \quad (70)$$

Accordingly, we can conclude that in the case of an empty conduit, the pressure gradient is:

- inversely proportional to the fourth power of the conduit diameter in the viscous term, and
- inversely proportional to the fifth power of the conduit diameter in the kinetic term.

Hence the empirical importance of measuring *accurately* the conduit diameter in experiments related to conduit permeability.

Finally, we point out that the viscous term in Equation (70) corresponds to Poiseuille's equation for laminar flow. Note, however, that by comparison, Poiseuille's equation has the

coefficient of π in the denominator, rather than the coefficient of 3 in Equation (70). Therefore, Poiseuille's equation *understates* the pressure gradient by 1 part in 22, a discrepancy of 4.55%, which falls within the measurement error of many typical engineering applications.

Let us now consider a quadratic relationship for the volumetric fluid flow, q , by expressing Equation (69) above, as follows:

$$aq^2 + bq + c = 0 \quad (71)$$

Where, b =a variable coefficient of q ; a =a variable coefficient of q^2 ; and c =a constant.

Rearranging Equation (71) gives:

$$aq^2 + bq = -c \quad (72)$$

Substituting ΔP for $-c$ in Equation (72) and rearranging gives:

$$\Delta P = aq^2 + bq \quad (73)$$

Solving Equation (73) for q gives:

$$q = \frac{-b \pm \sqrt{b^2 + 4a\Delta P}}{2a} \quad (74)$$

Let us define the coefficients a and b as follows:

$$a = \frac{8\delta^2 \lambda \rho_f L}{\pi^3 D^4 d_c} \quad (75)$$

$$b = \frac{1024\delta q \eta}{3D^2 d_c^2} \quad (76)$$

Substituting for a and b in Equation (73), we get Eq. (69):

$$\frac{\Delta P}{L} = \frac{1024\delta q \eta}{3D^2 d_c^2} + \frac{8\delta^2 \lambda q^2 \rho_f}{\pi^3 D^4 d_c}$$

In order to cross-reference with the conventional literature for packed conduits, we may now substitute for HQC variables as follows:

Substituting for d_c [Eq. (24)] and δ [Eq.(41)] in Equation (69), and rearranging gives:

$$\frac{\Delta P}{L} = \frac{1024(1-\varepsilon_0)^2 q \eta}{3D^2 d_c^2} + \frac{8(1-\varepsilon_0) \lambda q^2 \rho_f}{\pi^3 D^4 \varepsilon_0^6 d_c} \quad (77)$$

Switching the fluid flow parameter from volumetric flow rate to superficial velocity, we may now write:

$$\frac{\Delta P}{L} = \frac{256\pi(1-\varepsilon_0)^2 \mu_s \eta}{3\varepsilon_0^3 d_p^2} + \frac{(1-\varepsilon_0) \lambda \rho_f \mu_s^2}{2\pi \varepsilon_0^6 d_p} \quad (78)$$

Substituting for $256\pi/3=A$, on the left hand side of Equation (78), and $\lambda/(2\pi \varepsilon_0^3)=B$, on the right hand side of Equation (78), gives:

$$\frac{\Delta P}{L} = \frac{A(1-\varepsilon_0)^2 \mu_s \eta}{\varepsilon_0^3 d_p^2} + \frac{B(1-\varepsilon_0) \rho_f \mu_s^2}{\varepsilon_0^3 d_p} \quad (79)$$

We point out that Equation (79) corresponds to the general format of the Ergun equation. However, we call it the Q-modified Ergun equation because the “constants” of $A=268$ (approx.) and $B=\lambda/(2\pi \varepsilon_0^3)$, have been modified from Ergun's original constant values of 150 and 1.75 for A and B, respectively, and most importantly, B is *not a constant*, but rather is a *function* of both λ and ε_0 .

3. Results-Modeling the HQC as a Harmonic Oscillator

3.1. The Spatial Coordinates

We shall now return to the motion of the fluid within the HQC and describe it in terms of its instantaneous velocity coordinates in three dimensions, i.e., x, y, z.

Thus, we may write:

$$v = v_x + v_y + v_z \quad (80)$$

where, v =the total instantaneous velocity.

Let us define the *conduit* frictional time interval as follows:

$$t_0 = \frac{\pi D^2 L \varepsilon_t}{4q} \quad (81)$$

Where, t_0 =time to displace one conduit volume of fluid.

Let us define the *wall* shear stress as follows:

$$\tau_w = \frac{\Delta P D}{4L} \quad (82)$$

Where, τ_w =the wall shear stress.

Let us define the frictional fluid velocity as follows:

$$\mu_f = \sqrt{(\tau_w / \rho_f)} \quad (83)$$

Where, μ_f =the frictional fluid velocity.

Let us define the period of the fluid motion as follows:

$$T = \frac{2\pi}{\omega} \quad (84)$$

Where, T =the period of the fluid motion.

Let us define the frequency of the fluid motion as follows:

$$\phi = \frac{1}{T} \quad (85)$$

Where, ϕ =the frequency of the fluid motion.

Let us define the maximum displacement amplitude of the fluid motion as follows:

$$M_0 = \frac{d_c}{2} \quad (86)$$

Where, M_0 =the maximum displacement amplitude of the fluid motion (scale factor).

Let us define the instantaneous displacement amplitude as follows:

$$M = M_0 \exp(-\omega t_0) \quad (87)$$

Where, M =the instantaneous displacement amplitude of the fluid motion.

Note that the negative sign in the exponent in equation (87) represents the fact that the conduit wall frictional force acts in the opposite direction to the fluid motion and, hence, the motion is “damped” by wall friction.

Let us define the instantaneous displacement amplitude in the x-axis plane as follows:

$$x = M \cos P_Q \quad (88)$$

Where, x =the instantaneous fluid displacement amplitude in the x-axis plane.

Let us define the instantaneous fluid velocity in the x-axis plane as follows:

$$v_x = \frac{-M \lambda \sin P_Q}{\phi h} \quad (89)$$

Where, v_x =the instantaneous fluid velocity in the x-axis plane.

Let us define the instantaneous fluid acceleration in the x-axis plane as follows:

$$f_x = \frac{-M \lambda^2 \cos P_Q}{\phi h^2} \quad (90)$$

Where, f_x =the instantaneous fluid acceleration in the x-axis plane.

Let us define the instantaneous motion displacement in the y-axis plane as follows:

$$y = M \sin P_Q \quad (91)$$

Where, y =the instantaneous fluid displacement in the y-axis plane.

Let us define the instantaneous fluid velocity in the y-axis plane as follows:

$$v_y = \frac{M \lambda \cos P_Q}{\phi_h} \quad (92)$$

Where, v_y =the instantaneous fluid velocity in the y-axis plane.

Let us define the instantaneous fluid acceleration in the y-axis plane as follows:

$$f_y = \frac{-M \lambda^2 \sin P_Q}{\phi_h^2} \quad (93)$$

Where, f_y =the instantaneous fluid acceleration in the y-axis plane.

Let us define the instantaneous motion displacement in the z-axis plane as follows:

$$z = M \cos(\pi/4 - P_Q) \quad (94)$$

Where, z =the instantaneous fluid displacement in the z-axis plane.

Let us define the instantaneous fluid velocity in the z-axis plane as follows:

$$v_z = \frac{-M \lambda \sin(\pi/4 - P_Q)}{\phi_h} \quad (95)$$

Where, v_z =the instantaneous fluid velocity in the z-axis plane.

Let us define the instantaneous fluid acceleration in the z-axis plane as follows:

$$F_z = \frac{-M \lambda^2 \cos(\pi/4 - P_Q)}{\phi_h^2} \quad (96)$$

Where, f_z =the instantaneous fluid acceleration in the z-axis plane.

3. 2. The Hypothetical Q Unit Cell

We shall now describe the dimensionless manifestation of the fluid motion in the HQC which we term the "Hypothetical Q Unit Cell" (HQUC).

Let us define the *dimensionless* instantaneous motion displacement in the x-axis plane as follows:

$$x^* = \frac{x}{M_0} \quad (97)$$

Where, x^* =the dimensionless instantaneous fluid displacement in the x-axis plane.

Let us define the dimensionless instantaneous fluid velocity in the x-axis plane as follows:

$$v_z^* = \frac{v_z}{\mu_f} \quad (98)$$

Where, v_x^* =the dimensionless instantaneous fluid velocity in the x-axis plane.

Let us define the dimensionless instantaneous motion displacement in the y-axis plane as follows:

$$y^* = \frac{y}{M_0} \quad (99)$$

Where, y^* =the dimensionless instantaneous fluid displacement in the y-axis plane.

Let us define the dimensionless instantaneous fluid velocity in the y-axis plane as follows:

$$v_y^* = \frac{v_y}{\mu_f} \quad (100)$$

Where, v_y^* =the dimensionless instantaneous fluid velocity in the y-axis plane.

Let us define the dimensionless instantaneous motion displacement in the z-axis plane as follows:

$$z^* = \frac{z}{M_0} \quad (101)$$

Where, z^* =the dimensionless instantaneous fluid displacement in the x-axis plane.

Let us define the dimensionless instantaneous fluid velocity in the z-axis plane as follows:

$$v_z^* = \frac{v_z}{\mu_f} \quad (102)$$

Where, v_z^* =the dimensionless instantaneous fluid velocity in the z-axis plane.

4. Discussion-Exploring the QFFM

In order to further explore the implications of the HQC, we propose a series of worked examples which will articulate the role of the various parameters embodied in the QFFM. Our worked examples have the following *common* independent working variables: $D=0.46$ cm; $L=10$ cm; $\Omega_p=1.0$; $d_p=0.001$ cm; $\eta=0.01$ poise; and $\rho_f=1.0$ g/mL.

4.1. The HQC Fluid Current Normalization Coefficient λ

We begin with 8 worked examples involving an empty conduit having variable relative roughness (k_{dc}) values, as shown in Figures 13 and 14. They are as follows:

1. Empty conduit-smooth wall ($k_{dc}=0$)
2. Empty conduit-roughened wall ($k_{dc}=0.0001$)
3. Empty conduit-roughened wall ($k_{dc}=0.001$)
4. Empty conduit-roughened wall ($k_{dc}=0.01$)
5. Empty conduit-roughened wall ($k_{dc}=0.03$)
6. Empty conduit-roughened wall ($k_{dc}=0.05$)
7. Empty conduit-roughened wall ($k_{dc}=0.1$)
8. Empty conduit-roughened wall ($k_{dc}=0.5$)

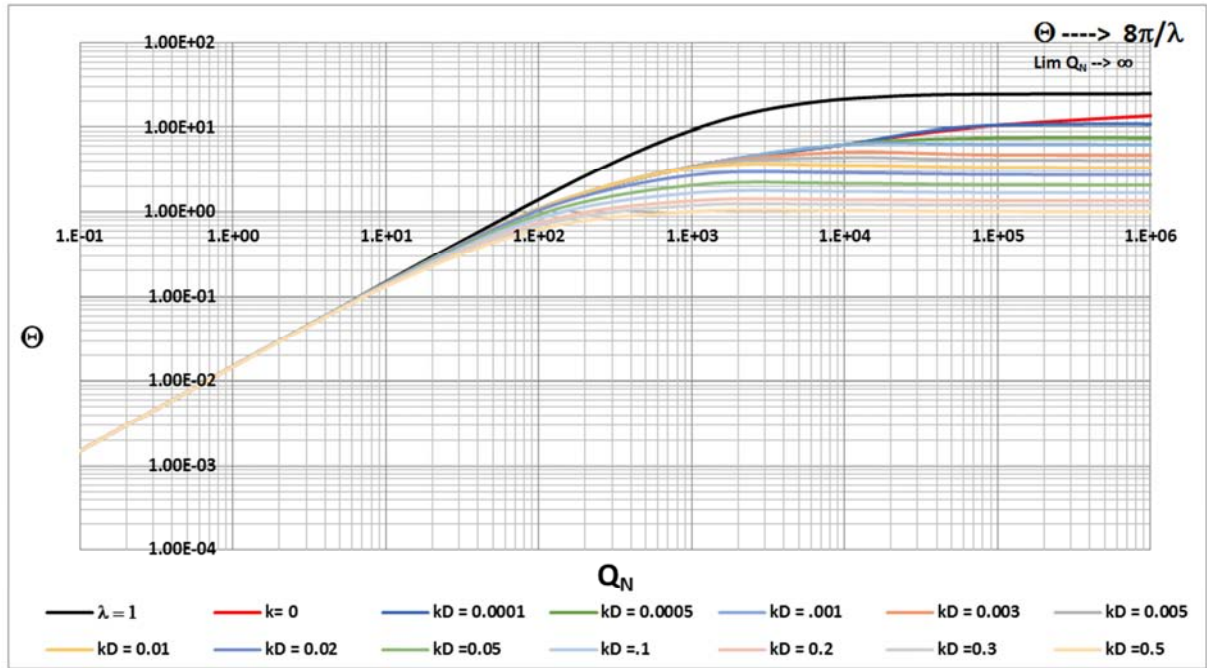


Figure 13. Dimensionless Permeability.

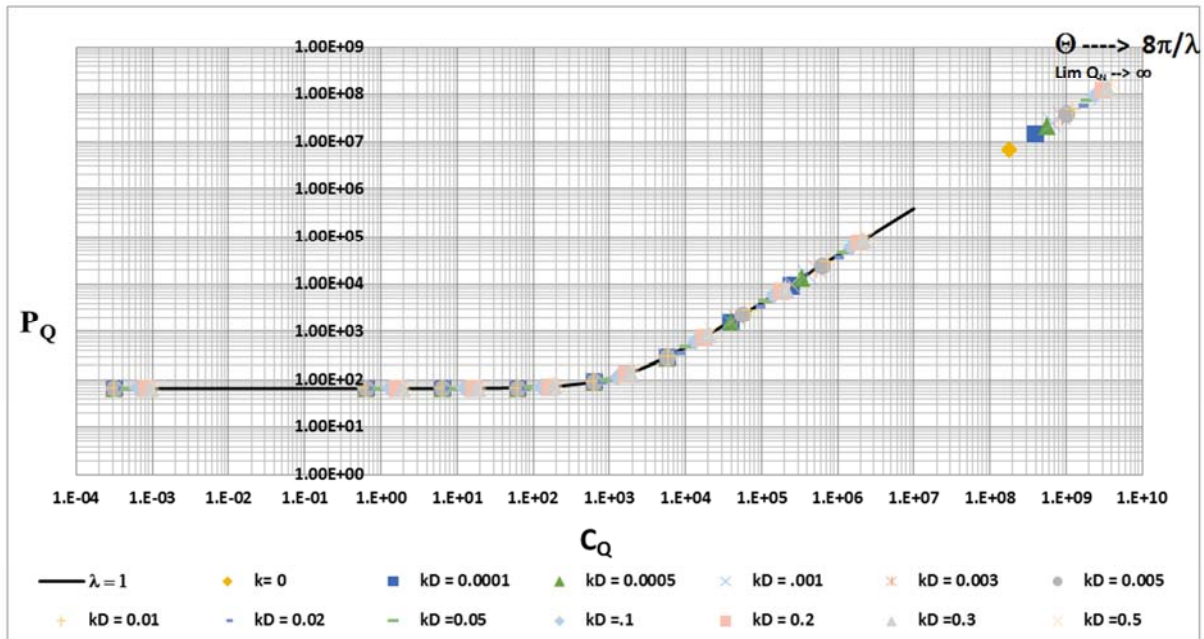


Figure 14. Viscous Friction Factor.

As shown in Figure 13, on a log-log plot of dimensionless permeability, Θ , versus fluid current, Q_N , the 8 worked examples produce characteristic dimensionless permeability line shapes, which vary according to the value of λ for each example, at high values of Q_N . There is no differentiation between these worked examples at low values of Q_N , because the wall roughness is buried beneath the wall boundary layer. Larger values of λ produce lower dimensionless permeability at high values of Q_N because the residual secondary wall effect is commensurate with the wall roughness coefficient.

On the other hand, as shown in Figure 14, also in a log-log format of P_Q versus C_Q , our typical graphical representation

of Quinn's Law for the same examples, the data yields a straight line whose intercept and slope are represented by the constants $k_1=64\pi/3$ and $k_2=1/8\pi$, respectively. Note that the exact location for each of the 8 examples on the x-axis of the plot is determined by the unique value of λ at each measured flow rate. We show the axis of this plot in a log-log format to highlight the relationship at the extremes of the values for wall-adjusted fluid current C_Q . The location of any given data point on the x axis for each worked example moves to higher values as a function of wall roughness, at comparable flow rates.

4.2. The HQC Tortuosity Coefficient τ

In our model, a packed conduit is the general case of the theory and an empty conduit a special case. They are differentiated in the theory, however, by virtue of the HQC tortuosity coefficient τ . This distinction is driven by the fact

that $\tau = \delta\gamma$, is a constant *less than unity* for an empty conduit (0.188) but is *greater than unity* and is *not* a constant for a packed conduit. In fact, for most practical packed conduits, the tortuosity factor is *enormous* by comparison to that of an empty conduit. We show a comparison in Figure 15 below.

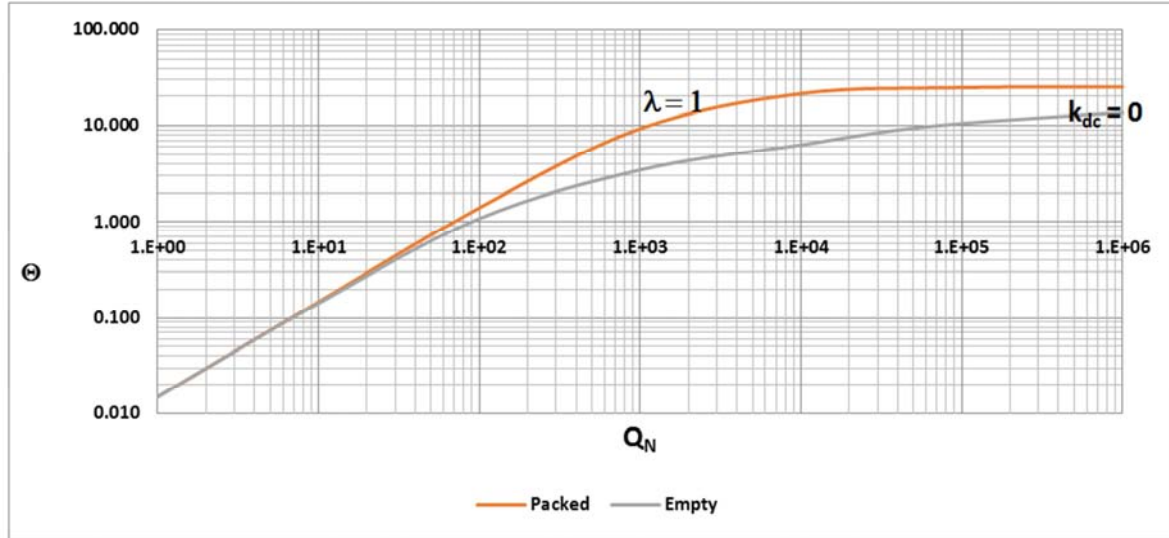


Figure 15. Impact of HQC Tortuosity.

HQC tortuosity manifests itself in the normalized boundary layer parameter, which we designate as the primary wall effect W_1 , and is best viewed on a plot of dimensionless permeability, Θ , versus fluid current, Q_N .

As shown in the plot, on the one hand, the normalized boundary layer in the packed conduit is infinitesimally thin, by virtue of the enormous tortuosity value, $\tau = 1.6 \times 10^9$, which means that the primary wall effect is negligible and, because the wall roughness is also negligible when $k=0$, there is no net wall effect. Consequently, for the packed conduit, the value of λ is close to the value of 1 for all values of Q_N , which results in the higher permeability line shown in the plot.

On the other hand, in the case of an empty conduit, in which the tortuosity value is extremely low, $\tau=0.188$, the boundary layer is wider at low values of Q_N and becomes

thinner as the value of Q_N increases. This results in a changing value of λ as a function of Q_N , which, in turn, produces the lower permeability line shown in the plot. At very large values of Q_N , however, the boundary layer is essentially completely dissipated ($\lambda=1$), in which case the dimensionless permeability of an empty conduit is identical to that of a packed conduit, when the HQC is hydraulically smooth ($k_{dc}=0$), and it approaches the upper limit value of 8π in the limit as Q_N tends to infinity.

Thus, the dimensionless permeability of an empty and packed conduit are different for a hydraulically smooth surface at low values of Q_N , but are identical in the limit as Q_N tends to infinity.

In addition, the value of λ also affects the time constant T , as shown in Figure 16 below, in the case of a packed conduit.

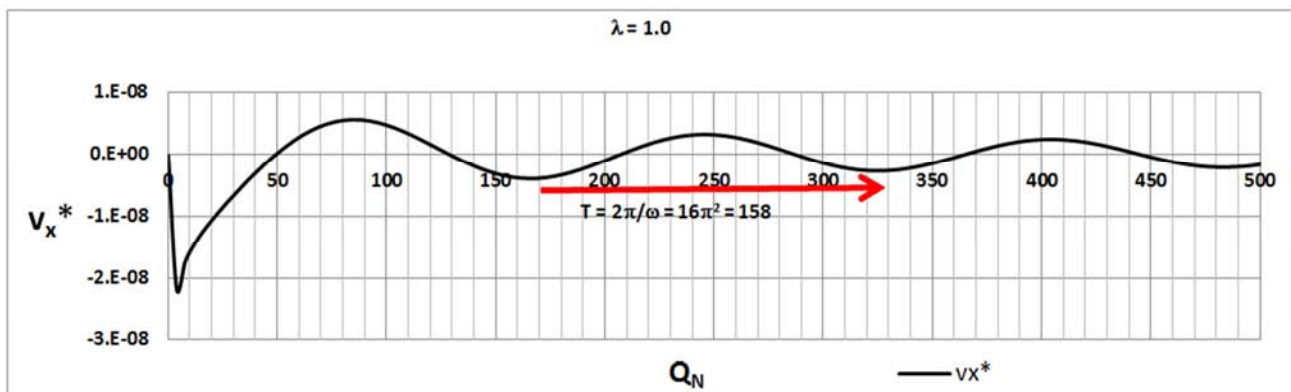


Figure 16. Velocity Profile-Packed Conduit.

As shown in Figure 16, the time constant T is represented by one full rotation of the fluid, which is shown on the x axis.

In the case of a packed conduit, the value of $T=158$. This represents the *maximum* time constant possible since it represents a λ value of unity, which, in turn, represents the *minimum* theoretical value of λ .

On the other hand, in the case of an empty conduit in which the value of λ maybe greater than 1, the value of the time constant T will always be less than that for a packed conduit, as shown in Figure 17 below.

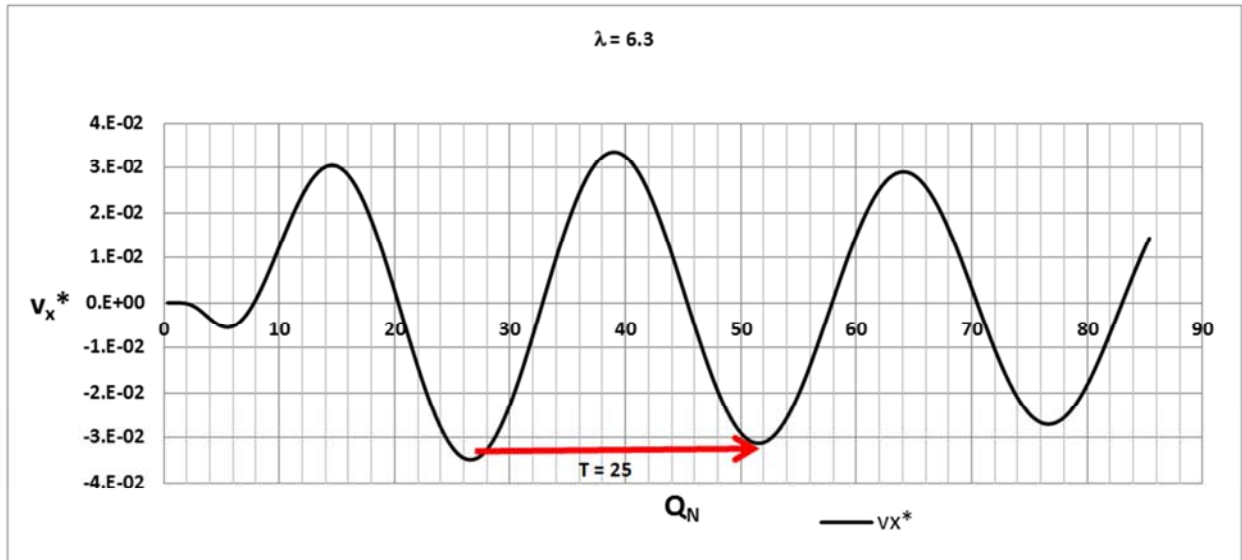


Figure 17. Velocity Profile-Empty Conduit.

As shown in the plot for an empty hydraulically smooth conduit, when the value of $\lambda=6.3$, the value of $T=25$. Of course, the value of λ will change at higher values of Q_N , as the boundary layer dissipates, which produces a corresponding increase in the time constant.

As is also apparent in Figures 16 and 17, the fluid motion is “damped” in two ways; firstly, by *wall friction*, which is apparent at low values of Q_N , when wall friction has its major impact and, secondly, by *fluid friction*, which becomes

increasingly dominant with higher values of Q_N .

4.3. The HQC Net Wall Effect W_N

In our theoretical model, we begin with a description of the wall effect by focusing on our definition for the dimensionless boundary layer, β_0 . As shown in Figure 18 below, the boundary layer varies from a value of unity at low values of Q_N to a value approaching zero at high values of Q_N .

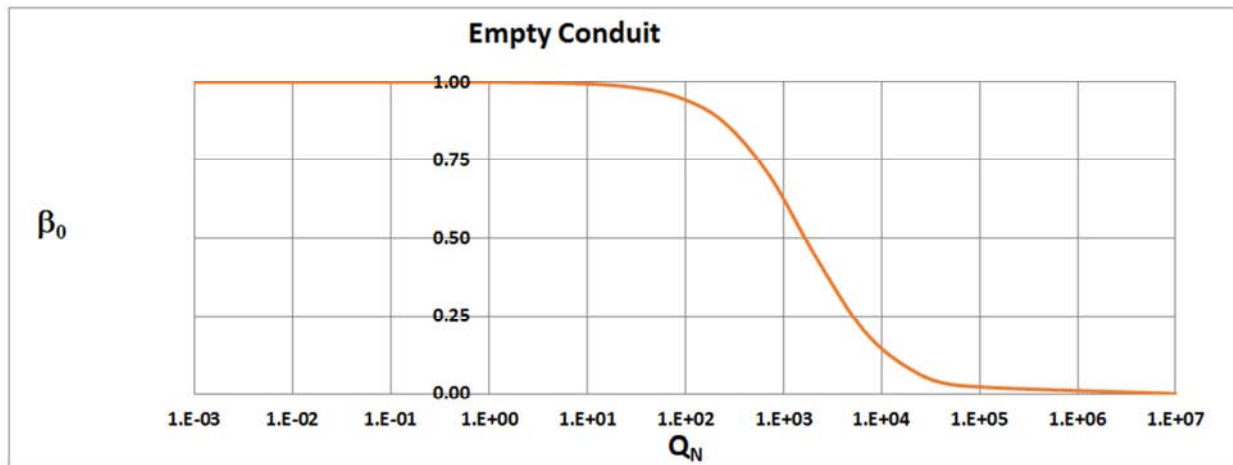


Figure 18. HQC Dimensionless Boundary Layer β_0 .

The characteristic shape in this plot underlies the fluid current changes from having fluid *current-velocity streamlines* parallel to the walls of the channel (laminar flow), at low values of Q_N , to those which are more concentric with the center point of the channel, at high values of Q_N (turbulent flow). This change in the fluid flow profile

characteristics from parabolic in nature to more circular in nature disrupts the boundary layer, which, in turn, becomes progressively thinner as the value of Q_N increases. It is the value of the fluid current, Q_N , which produces the rotational component in the fluid current. More rotation at higher values of Q_N reduces the thickness of the boundary layer.

Next we consider the HQC *primary* wall effect, W_1 , shown in Figure 19 below.

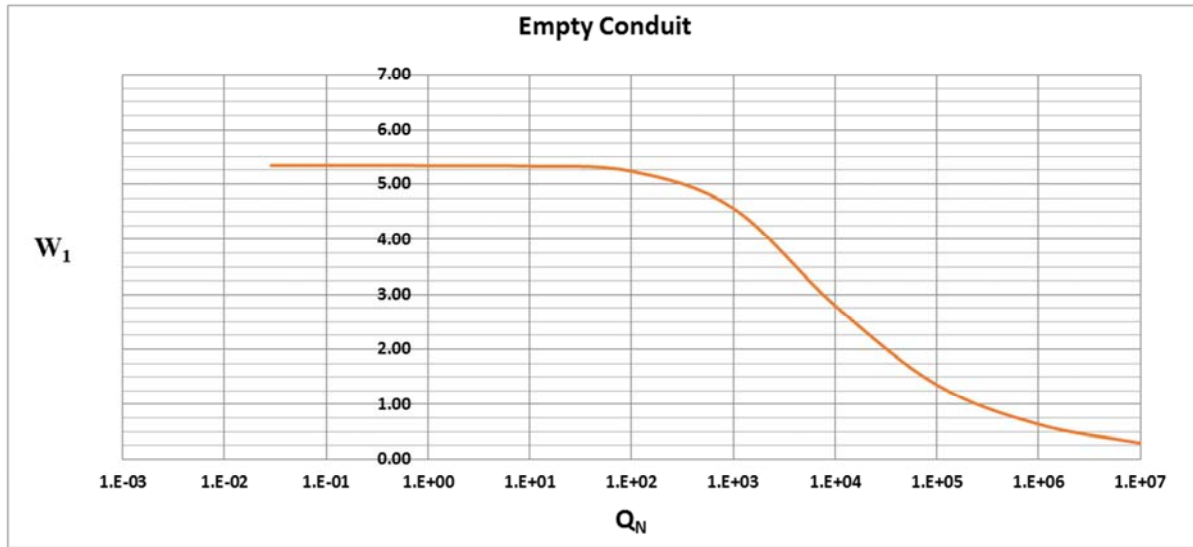


Figure 19. HQC Primary Wall Effect.

As shown in the plot, the primary wall effect is the boundary layer normalized for fluid channel tortuosity. Accordingly, in the case of an empty conduit (shown here) in which the tortuosity coefficient is less than unity, the primary wall effect is enhanced. For instance, in the example shown in the plot for an empty conduit, the normalized boundary layer is increased from unity, for the un-normalized boundary

layer, to approximately 5.5. In contrast to an empty conduit, however, the primary wall effect in the case of a packed conduit is virtually negligible because the tortuosity coefficient is typically *very, very large*.

We now proceed to evaluate the HQC *secondary* wall effect, W_2 , as shown in Figure 20 below.

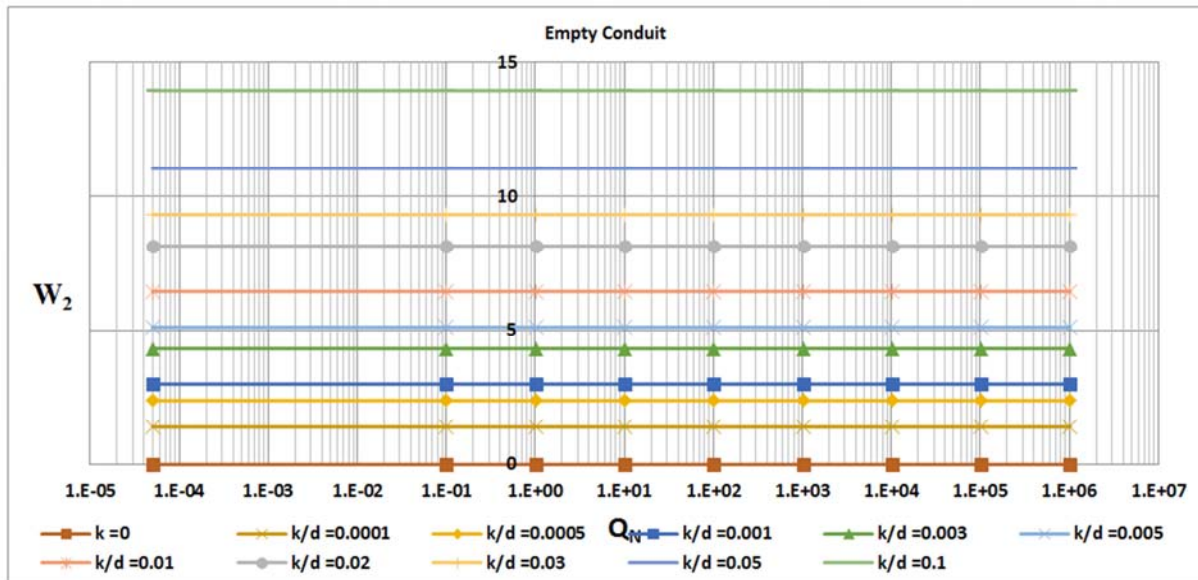


Figure 20. HQC Secondary Wall Effect.

As shown in the plot, the secondary HQC wall effect, W_2 , is simply the degree of relative roughness on the inner channel wall. It increases as the relative roughness coefficient increases and is constant for a given value of the wall relative roughness coefficient, k_{dc} , throughout the entire fluid flow

regime from low to high values of Q_N .

Next we identify the *residual* secondary wall effect, Q_{2R} , which is the degree to which the relative roughness coefficient “punches through” the normalized boundary layer. This is shown in Figure 21 below.

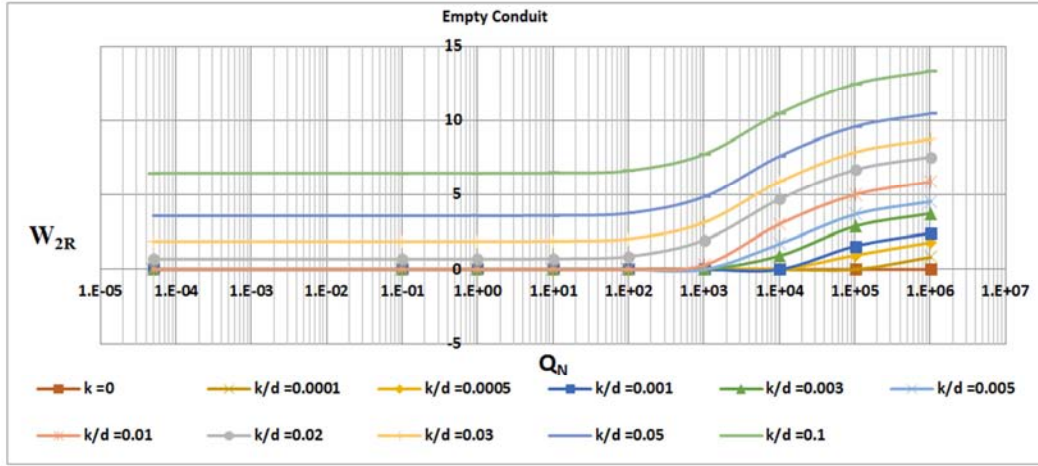


Figure 21. HQC Residual Secondary Wall Effect ($W_2 - W_1^{1.2}$).

As shown in the plot, the secondary wall effect is masked by the normalized boundary layer at low values of Q_N where the boundary layer is thickest, and gradually becomes more dominant, as it protrudes beyond the boundary layer at higher values of Q_N .

Next we evaluate the HQC net wall effect, W_N , as shown in Figure 22 below.

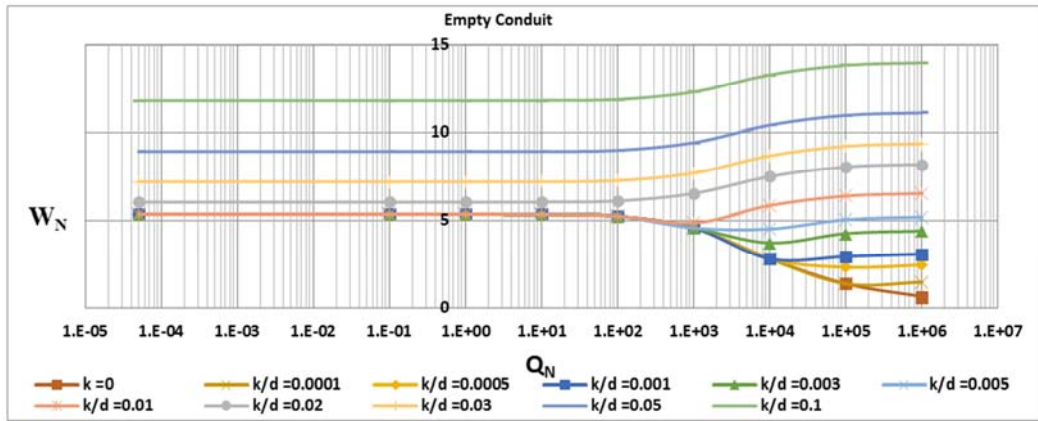


Figure 22. HQC Net Wall Effect ($W_1 + W_{2R}$).

As shown in the plot, the net wall effect, W_N , is the sum of the primary, W_1 , and residual secondary, W_{2R} , wall effects. Note that the normalized boundary layer is apparent in this plot at low values of Q_N .

Finally, we evaluate the influence of the HQC net wall effect, W_N , on the HQC fluid current. This we accomplish by showing a plot of the HQC fluid current normalization coefficient, λ , versus the fluid current, Q_N , in Figure 23 below.

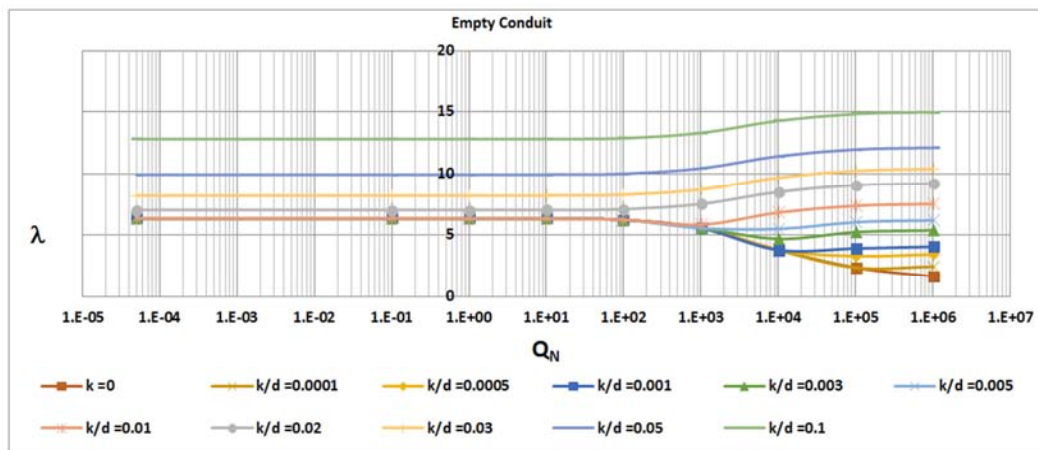


Figure 23. HQC Fluid Current Normalization Coefficient λ .

As shown in the plot, the normalized fluid current is relatively constant at low values of Q_N and reaches a plateau which may be greater or less than the primary wall effect, commensurate with relative wall roughness.

4.4. The Fluid Current-Velocity Streamlines

When the pressure gradient is unidirectional, as is the case in a walled conduit, the flow only occurs in the direction of the pressure gradient. We can show this by using Math WorksTM in MatLabTM software to plot the motion of the fluid as shown in Figure 24 below.

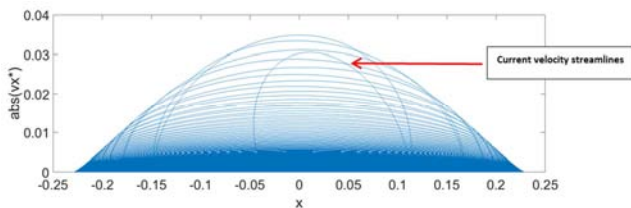


Figure 24. Q-Fluid Current-Velocity Streamlines.

As shown in Figure 24, the scale of the motion is defined by the diameter of the HQC, i.e., d_c . In this example of an empty conduit, the diameter of the HQC is 0.46 cm and, accordingly, the maximum radius of the fluid flow profile is $x=0.23$ cm. Note that the instantaneous speed is zero at both conduit walls ($x=0.23$ cm, and $x=-0.23$ cm), i.e., the no slip boundary condition and reaches its maximum value in the center of the channel ($x=0$ cm). The flow velocity profile goes from a *parabolic* type shape at low values of the fluid current $Q_N(t)$ to almost flat at the highest values of $Q_N(t)$. Accordingly, we refer to the velocity lines displayed as “current-velocity streamlines”.

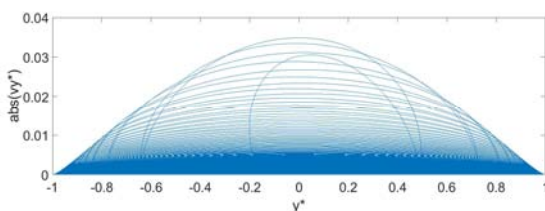


Figure 25. Q-Fluid Current-Velocity Streamlines.

As shown in Figure 25, the dimensionless fluid flow profile has the normalized radius of unity as shown in the plot of $\text{abs}(v_y^*)$ versus y^* .

In the case where the pressure gradient is not unidirectional, we can view the fluid velocity profile in the x axis plane, as in Figure 26 below.

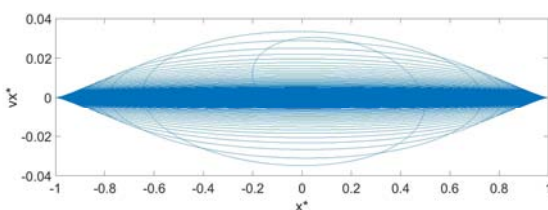


Figure 26. Q-Fluid Current-Velocity Streamlines.

As shown in Figure 26, the instantaneous fluid speed is zero at the wall and maximum in the center of the channel. In addition we can see the parabolic motion changing as a function of the value of the Q_N number. In this plot, the Q_N number increases towards the center from the top and bottom edges of the velocity streamlines.

We can also view the velocity profile in three dimensions, as shown in Figure 27 below.

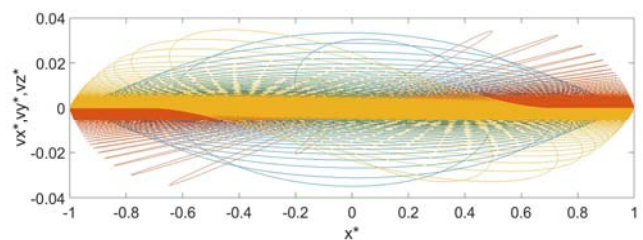


Figure 27. Q-Fluid Current-Velocity Streamlines.

As shown in Figure 27, the flow profile takes on the characteristic shape shown in the plot.

Similarly, we can view the fluid velocity profile as a function of fluid current, Q_N , in the three dimensional plane as shown in Figure 28 below.

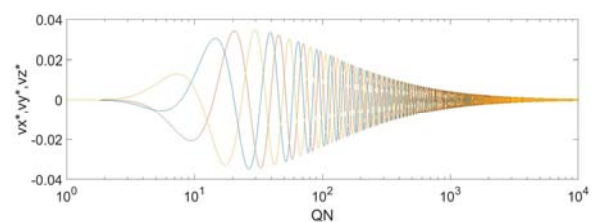


Figure 28. Fluid Velocity Profile.

As shown in the plot, the changing fluid flow profile is captured as a function of fluid current using a log x axis. The damping effect of wall friction and fluid friction are apparent in this plot. Note that the amplitude of the wave initially increases due to the wall effect. Having reached its maximum, it then decreases as the internal fluid friction becomes more dominant.

Next we view the instantaneous dimensionless boundary layer as a function of Q_N , as shown in Figure 29 below.

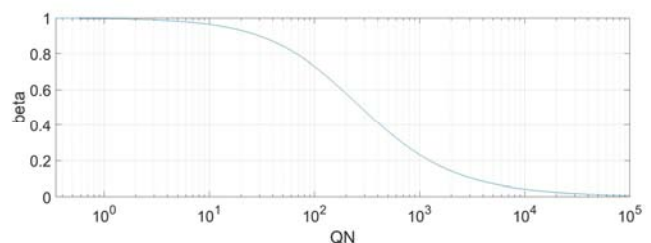


Figure 29. Boundary Layer Profile.

In Figure 29 we can see the disruption of the fluid wall boundary layer as it goes from unity, at low values of Q_N , to zero at very high values of Q_N , on a log x axis.

We can view the important dimensionless parameters of β , P_Q and Θ , as a function of Q_N , in a log-log plot, as shown in Figure 30 below.

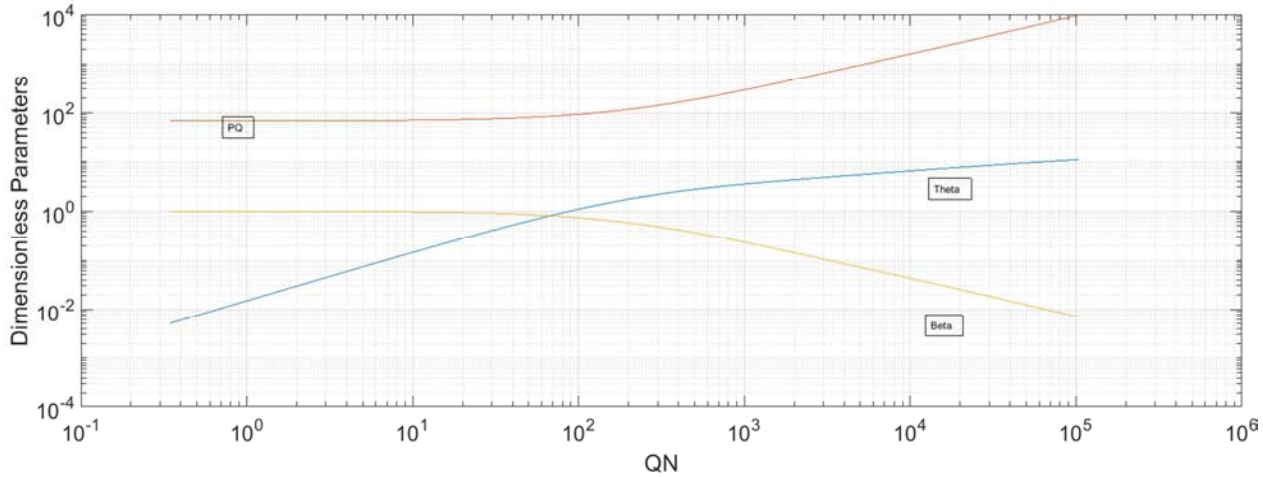


Figure 30. HQC.

In Figure 30 we can see how these dimensionless parameters mirror one another, using a log scale on both axes.

In a dimensional manifestation of scale, we can view the thickness of the boundary layer in Figure 31 below.

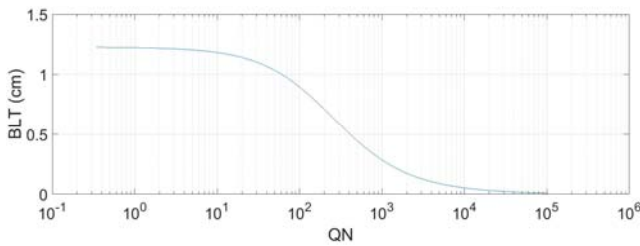


Figure 31. Boundary Layer Thickness Profile.

As shown in Figure 31, the thickness of the wall boundary layer decreases as a function of Q_N .

We can also view the fluid motion in terms of the three parameters of BLT, x^* and Q_N , as shown in Figure 32 below.

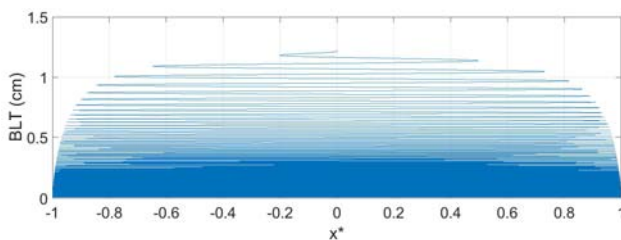


Figure 32. HQC.

Note that at very low flow rates, the boundary layer consumes almost the entire channel diameter, as shown in Figure 32.

The boundary layer thickness is equivalent to the radius of the HQC at time zero, i.e., when the fluid is at rest. Fluid motion begins in the center of the HQC and gradually spirals outward as a function of the fluid current, Q_N . The boundary layer thickness is minimized at the maximum value of Q_N

reached in any given experiment. Accordingly, one can think of the Q_N parameter as a “fourth dimension” when viewing the fluid velocity profile, representing as it does, the movement of elapsed time of the harmonic oscillator.

4.5. “aminar”, “Transitional”, “Turbulent” and “Chaos”

Finally, the issue of fluid chaos as articulated in many conventional scholarly works demands attention in light of the QFFM [Southernland]. The theory outlined herein contradicts the conventional wisdom that fluid turbulence is merely fluid velocity occurring in a random and unpredictable fashion. On the contrary, the QFFM demonstrates that fluid current is in fact highly structured and totally predictable. We underscore this point in Figure 33 below.

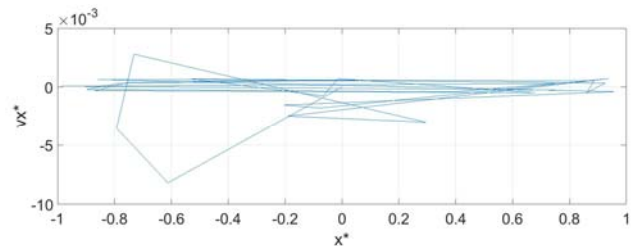


Figure 33. Fluid Flow Profile.

As shown in Figure 33, we include a plot of the exact same data as that presented in Figure 26.

The data shown in Figure 26 has a flow rate domain in MatLab™ of q : 0.01; 0.001; 300. In layman's terms, this means that the flow rate varies between a value of 0.01 mL/sec and 300 mL/sec and that there is a data point recorded every 0.001 mL/sec, i.e., the *measurement interval* is 0.001 mL/sec.

The data shown in Figure 33, on the other hand, has a flow rate domain of q : 0.01; 10; 300, i.e., the same range of flow rates but a much *larger* flow rate interval. Actually the flow rate interval is $10/0.001=10,000$, i.e., 10,000 times larger.

The explanation, therefore, for the “chaotic” view of the fluid instantaneous velocity in Figure 33, as opposed to the “highly structured” view of the fluid profile in Figure 26, for the exact same data, is due to the fact that there are not enough data points taken in the plot in Figure 33 to identify the precise motion of the fluid, noted above, the period of the motion in a packed conduit is approximately 158 ($T=2\pi/\omega$, and $\lambda = 1$; $T = 16\pi^2 = 158$ approximately).

In Figure 26 the interval of 0.001mL/sec provides ample data points to clearly outline the motion of the fluid, since this interval represents a “slice” in dimensionless time, (ΔQ_N) much smaller than the period of the motion ($Q_N=158$).

Accordingly, the conventional folklore labels of, “Laminar”, “Transitional”, “Turbulent” and “Chaotic flow” do not represent scientifically defensible criteria. Rather, they are merely *subjective experimental observations* which have never been quantified to any *scientifically acceptable standard*. Among other things, this is why the fluid dynamic landscape is littered with equations and proclamations which purport to set boundaries around each of these ill-defined labels and, consequently and unsurprisingly, none of the proposed boundaries have found universal acceptance. On the other hand, the QFFM replaces all these subjective labels with just one entity “fluid current” and defines it with scientific precision and accuracy. Moreover, it postulates that fluid current is a *continuum* valid throughout the entire range of flow regimes and, when evaluated with the necessary precision in the *fourth* dimension, i.e., the interval values of ΔQ_N , commensurate with the flow embodiment which surrounds it, is highly quantifiable and predictable.

5. Validation of the QFFM and Quinn’s Law

We begin our validation protocol by focusing on the general case of our hypothetical Q channel, the packed conduit. In so doing, we have chosen measured data from 4 third party published studies and 3 from homegrown experiments. The homegrown experiments were necessary to augment the other studies in order to cover the region of higher Q_N values, where no third party published studies were available.

5.1. Packed Conduits Farkas, et al

In a 1999 publication by Farkas, Zhong and Guiochon, entitled Validity of Darcy’s Law at Low Flow Rates in Liquid Chromatography [29, 30], Farkas and his co-authors report the results of some very exacting measurements which they made to validate Darcy’s law. Using a column containing spherical particles packed to a *measured* external column porosity of 0.399, (Figure 2 in the paper), the authors *measured* the column pressure drop *and fluid flow rate* at flow rates ranging between 0.015 and 0.5 mL/min with ethylene glycol as the fluid. They state that the particles in the column are spherical and appear to have gone to extraordinary lengths to obtain an accurate measure of the particle diameter and, of course, as a result of modern

techniques of particle size classification, the particle size distribution is narrow. Moreover, they used the technique of inverse size exclusion chromatography to determine the external column porosity which is a very accurate methodology *when used in the manner described by these authors for the column under study in this paper*.

The range of modified Reynolds number covered by the measurements in this paper, 5×10^{-5} to 5×10^{-3} , is so low that we consider it to be not only unique in the literature on bed permeability, but also the most relevant data available pertaining to laminar flow in closed, packed-bed conduits. The authors accomplished this feat by choosing the combination of a high viscosity fluid (ethylene glycol), small spherical particles (10 micron approx.) and low superficial fluid velocity, a consequence of their choice of column diameter in combination with fluid volumetric flow rates.

Coulson

The PhD thesis of J. M. Coulson, published in 1935 contains 111 pages of single-spaced text and tables, as well as approximately a dozen pages of engineering drawings and hand-plotted graphs [31].

The study involves 10 packed columns of varying particle sizes and porosities. All the particles are perfectly spherical, steel, non-porous ball bearings ranging in diameters from the smallest at 1/16 inch (approx. 1600 micron) to the largest 5/16 inch (approx. 8,000 micron).

The column hardware assembly consisted of a series of 2-inch internal-diameter brass castings, honed to a high finish, and bolted together to form a single column of nine sections. Glass U-tube manometers were mounted at the section interfaces to measure pressure drop. The manometers were arranged in a rather complex way using air as a pressurization counterbalance and, depending upon the pressure drop ranges, the U-tubes were filled with either mercury or water. The same column hardware assembly was used for each of the packed columns.

The pressure source was an adjustable weir assembly which moved in a vertical plane thus applying head pressure by virtue of its relative elevation to the column inlet. A circulating pump was used to recycle the effluent back to the weir. The fluid was light oil with a kinematic viscosity of approximately 1 stokes.

Flow rate measurements were taken on a gravimetric basis and the time of displacement was measured by stopwatch. The column length was measured, as was the mass of spheres used for each bed compaction. The mass of each sphere was measured and the volume occupied by the spheres was thus calculated. The column porosity was calculated by subtracting the volume occupied by the spheres from the empty column volume which was calculated from the physical dimensions of the cylinder (column).

The viscosity of the fluid was determined for each measurement by measuring the temperature of the fluid and reading the corresponding viscosity from a temperature/viscosity curve obtained by a Redwood viscometer. Density measurements were taken for each experiment by collecting a sample of the fluid effluent and

measuring the density in a hydrometer.

Ergun

Sabri Ergun et al published three seminal papers circa 1950 [32, 33, 34, 35]. In the last of these papers, 1952, Ergun published his now famous Ergun equation which he says was based upon a data base of 640 measurements in packed columns. In all three papers, he included much experimental data, some of which he carried out himself and some of which he took from third party studies. In this paper, we focus on the measurements he made himself for columns which contained both spherical and irregular particles through which he passed nitrogen gas. We include in our selected data base approximately 70 different columns with about 8 individual flow rate measurements for each column. Thus, our data base represents more than 500 individual measurements. All the measurements are in the transitional region of the fluid flow regime, which means that all his pressure drop measurements contained significant contributions from both viscous and kinetic sources.

Giddings

We include as part of our validation the works of J. C Giddings included in his Table 5.3-1 reported on page 209 of his 1965 textbook [36]. This reported data includes permeability measurements of packed chromatographic columns containing both nonporous and porous particles. Importantly, Giddings took advantage of smooth spherical glass bead particles to overcome the difficulty associated with irregular particle shape.

HMQ-1

The column used in this study was a chromatographic column prepared by this author by means of slurry packing under a packing pressure of 5,000 psi approximately, a technique well known in the chromatographic field. The column was made of 316 SS and had the dimensions of 2.1mm in diameter and 100 mm in length. The particles were made of an organic copolymer which was cross-linked to give the particles sufficient rigidity to be run at pressures up to several hundred bars. The particles are known by the commercial name of Oasis and are manufactured by Waters Corporation. The particle size distribution was measured by standard coulter counter analysis and had an average particle size of 30 micron. In addition, the particle size distribution was narrow. External porosity was measured in dichloromethane solvent by inverse size exclusion chromatography and determined to be 0.463. Pressure drop measurements were taken in the same fluid, dichloromethane, and the flow rate was set using a pre-calibrated HPLC constant flow rate pump with flow rate and pressure drop data recorded in a flow rate range of 1 to 10 mL/min. This combination of experimental variables

provided a range of modified Reynolds numbers of 1 to 8 approximately, which corresponds to the transition region of the flow regime.

HMQ-2

The column used in this study was a chromatographic column, dry packed by this author using the well-known tap and vibrate method of column packing. The column was made of 316 SS and had the dimensions of 1.002cm in diameter and 248 cm in length. The particles were made of an inorganic rigid substrate, non-porous glass beads and were purchased from the Shot glass company. They were spherical in shape as well as smooth and nonporous. The particle size distribution was measured by calibrated calipers in conjunction with microscopy and had an average particle size of 1,000 micron. In addition, the particle size distribution was narrow. The physical size of this column was chosen such that it had a large empty column volume (196 mL) which enabled the measurement of external porosity by volumetric means. External porosity was measured by filling the already dry-filled column with water and measuring the volume (76 mL) with a graduated cylinder. Its external porosity value was thus 0.39. Pressure drop measurements were taken in water and the flow rate was set using a pre-calibrated HPLC constant flow rate pump with flow rate and pressure drop data recorded in a flow rate range of 4 to 500 mL/min.

This combination of experimental variables provided a range of modified Reynolds numbers of 1 to 175 approximately, which corresponds to the transition region of the flow regime.

HMQ-4

The column used in this study was made of 316 SS and had the dimensions of 1.07cm in diameter and 40.6 cm in length. The particles were made of electro-polished stainless steel ball bearings and were spherical in shape as well as smooth and nonporous. The particle size distribution was measured by calibrated calipers and had an average particle size of 0.952 cm. Because the particles were just slightly smaller than the column diameter, it was easy to count the number of particles required to fill the column. A total of 41 particles filled the column and this resulted in a column external porosity of 0.488. Pressure drop measurements were taken using air as the fluid medium and a very sensitive calibrated pressure transducer. The flow rate was provided by a calibrated constant volume gas syringe pump used for experiments related to human lung performance. This combination of experimental variables provides a range of Q_N values of 1×10^{-4} to 1×10^5 , a total range of 9 orders of magnitude, which range represents sufficient values to establish the overall shape of the plotted curve of Θ v Q_N .

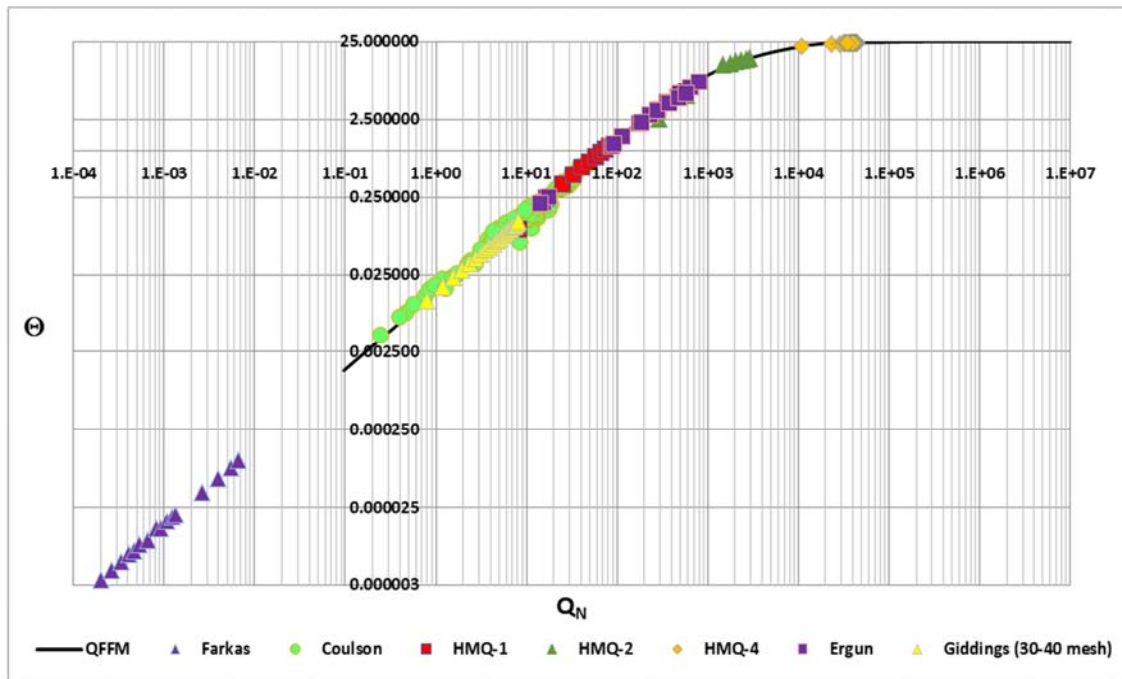


Figure 34. Quinn's Law Validation-Packed Conduit.

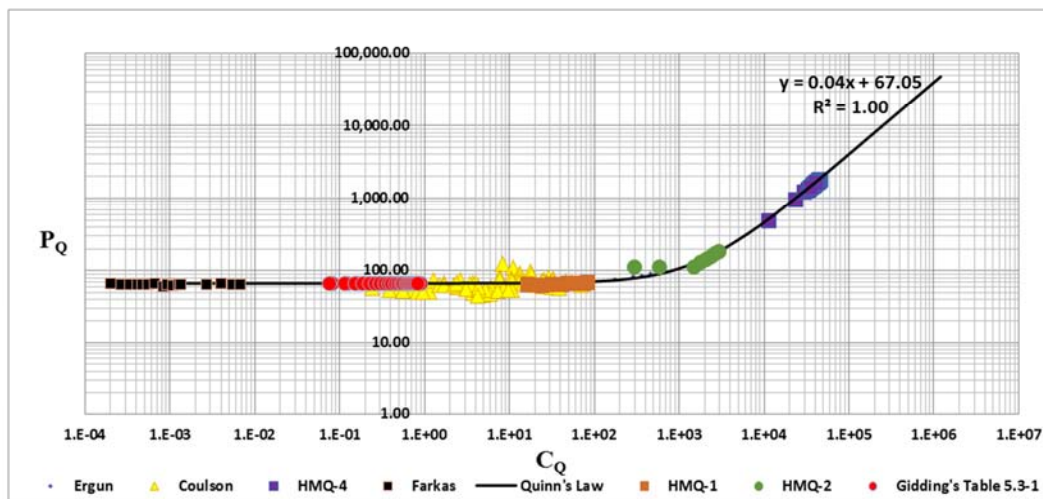


Figure 35. Quinn's Law Validation-Packed Conduit.

As shown in Figures 34 and 35, the empirical data for this data set of packed conduits fits extremely well to the theoretical curve for the QFFM as well as for Quinn's Law, for all measured data.

5.2. Empty Conduit-Smooth Walls

The Princeton Study

What we call "The Princeton Study" herein is a compilation of two papers published between 2004 and 2005 [37, 38]. The 2005 paper contains a brief abstract which we repeat herein; "The friction factor relationship for high-Reynolds-number fully developed turbulent pipe flow is investigated using two sets of data from the Princeton Super pipe in the range $31 \times 10^3 \leq Re_p \leq 35 \times 10^6$. The constants of Brandt's 'universal' friction factor relationship are shown to be accurate over only a limited Reynolds-

number range and unsuitable for extrapolation to high Reynolds numbers. New constants, based on a logarithmic overlap in the mean velocity, are found to represent the high-Reynolds-number data to within 0.5%, and yield a value for the von Karman constant that is consistent with the mean velocity profiles themselves. The use of a generalized logarithmic law in the mean velocity is also examined. A general friction factor relationship is proposed that predicts all the data to within 1.4% and agrees with the Blasius relationship for low Reynolds numbers to within 2%".

The Oregon Study

The Oregon study can be found in a 2002 publication by Oregon University scientists [39]. The paper contains a brief abstract which we repeat herein; "We demonstrate that an

unusually small pipe flow apparatus using both liquid helium and room temperature gases can span an enormous range of Reynolds numbers. This paper describes the construction and operation of the apparatus in some detail. A wide range of Reynolds numbers is an advantage in any experiment seeking to establish scaling laws. This experiment also adds to evidence already in hand that the normal phase of liquid helium is a Navies-Stokes fluid. Finally, we explore recent questions concerning the influence of molecular motions on the transition to turbulence (Muriel 1998) and are unable to observe any influence”.

The Nikuradze Smooth Wall Data

The data in this study is taken from a *circa* 1930 paper by J. Nikuradse [40]. The study involved the flow of turbulent water through “smooth” test pipe sections of drawn brass construction and unspecified inner wall finish. The range of Reynolds number studied reached as high as one million approximately. Pipe diameters ranging from 1 to 10 cm were studied. The data lies in the region of fully developed turbulent flow for the most part.

5.3. Homegrown Experiments in Empty Conduits-Smooth Walls

In order to supplement our validation using third party published data with our own homegrown experiments, we carried out a series of measurements in empty capillaries [41]. In every experiment, we measured the temperature, flow rate and pressure drop at as many flow rates as was reasonably possible given the constraints of the pump, i.e. maximum pressure, minimum flow rate and pump power. The pressure drop was recorded by means of a calibrated pressure transducer purchased from Omega, Model # PX409-250DWU5V. It had a pressure range of 0-250 psi and ran under a 24V DC power supply. The flow rate was measured for each recorded pressure drop by means of a stop watch and graduated cylinder. The time interval over which the measurement was taken varied with the flow rate-larger for low flow rates and smaller for high flow rates. The temperature of the fluid was recorded by means of a thermocouple purchased from Omega, Model # TCK-NPT-72.

The liquid pump was manufactured by Fluid-o-Tech (Italy), Model # FG204XDO (P. T) T1000. It is an external gear pump, 0-5V, 300-5,000 rpm delivering *pulseless* flow rate under a constant pressure. The flow rate of the pump was controlled by means of a laptop computer running under a software control package manufactured by National Instruments. The pump had a flow rate range of 100-1600 mL/min and a pressure maximum rating of circa 200 psi. This range of flow rates was further enhanced at lower flow rate values by the use of our recycle valve, which was used to shunt the flow between the device under study and the recycle line.

HMQ-10

In this experiment, we chose to evaluate the permeability of a commercially available empty capillary made of Peek plastic, an article of commerce in the HPLC industry, which had a nominal diameter of 0.02 inches. The fluid used was water and we chose to evaluate two different lengths, 100 cm and 726 cm, in order to be able to exploit different modified Reynolds number ranges of values.

HMQ-11

In this experiment, we chose a Peek capillary of nominal diameter 0.03 inches and lengths of 100 and 700 cm. In this experiment we also included in our measurements two different fluids, water and Glycol. The viscosity of the water was 0.01poise and the density was 1.0 g/mL. The viscosity for the Glycol solution was 0.38poise and the density was 1.14 g/mL.

HMQ-12

In this experiment, we chose a stainless steel capillary of nominal diameter 0.07 inches x 66.5 cm in length. We used both water and glycol as the test fluids.

HMQ-13

In this experiment, we chose a stainless steel capillary of nominal diameter 0.08 inches x 31.75 cm in length using, again, both water and glycol as the test fluids.

This compilation of measured data provides a range of Q_N values of 1×10^{-1} to 4×10^6 , a total range of 7 orders of magnitude, which range represents sufficient values to establish the overall shape of the plotted curve of $\Theta \propto Q_N$.

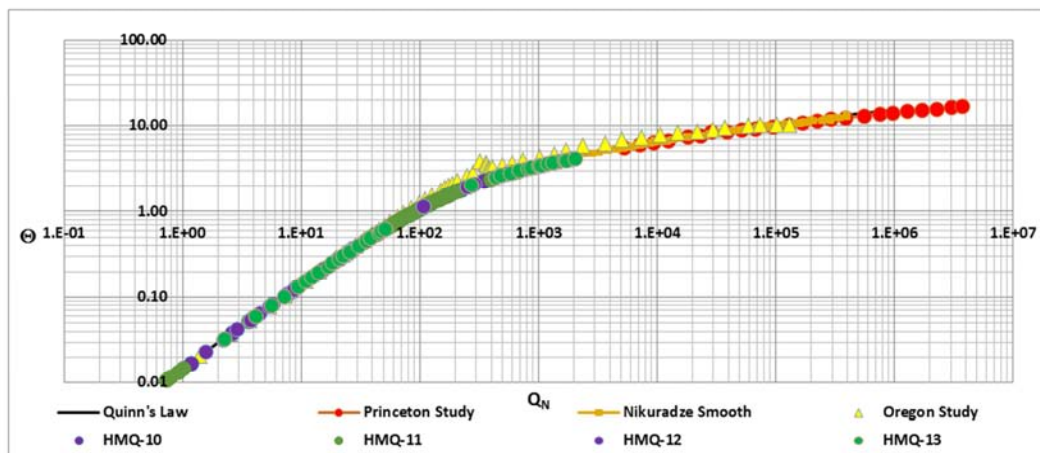


Figure 36. QFFM Validation-Empty Conduit Smooth.

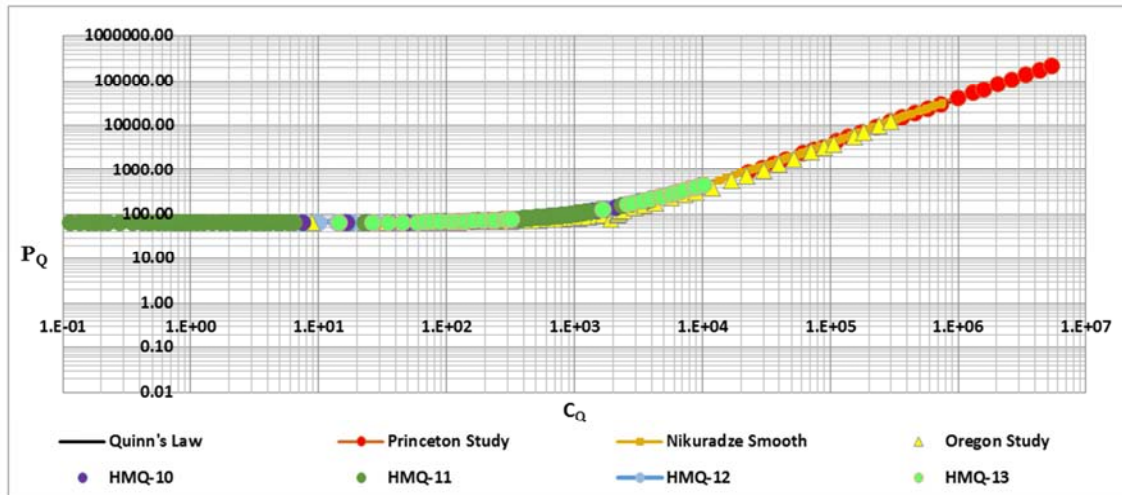


Figure 37. Quinn's Law Validation-Empty Conduit Smooth.

As shown in Figures 36 and 37, the empirical data for the smooth empty conduits evaluated, fits extremely well to the theoretical curve for the QFFM as well as for Quinn' Law, for all measured data.

5.4. Empty Conduits-Roughened Walls

Nikuradze Data

The data in this study is taken from a *circa* 1933 paper by J. Nikuradze [42]. The study involved the flow of turbulent water through pipes consisting of drawn brass tubes the inner walls of which were roughened by the deposition of particles

of sand. The range of Reynolds numbers studied reached as high as one million approximately. Pipe diameters ranging from 2 to 10 cm were studied using varying degrees of inner wall roughness. This study is considered the gold standard against which all roughened pipe data is compared.

The combination of experimental variables involved in this study provides a range of Q_N values of 5×10^1 to 2×10^5 , a total range of 6 orders of magnitude, which range represents sufficient values to establish the overall shape of the plotted curve of Θ versus Q_N [See Figure 38].

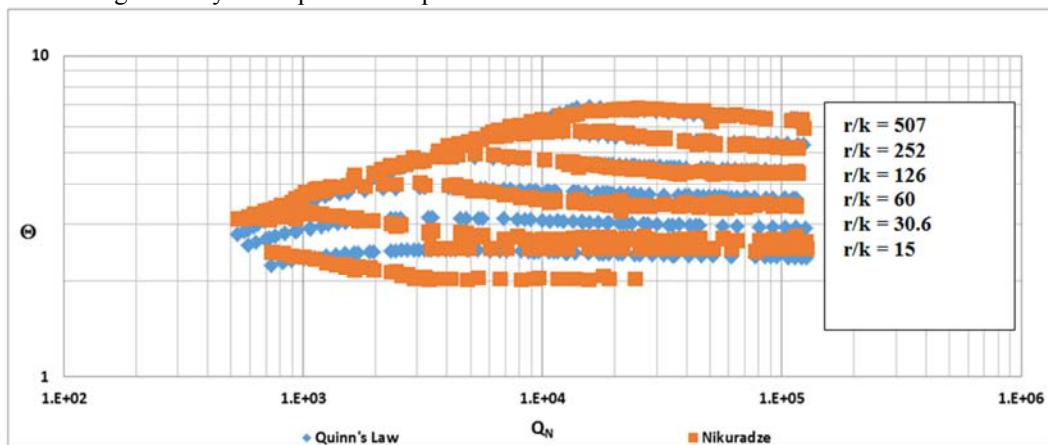


Figure 38. QFFM Validation-Empty Conduit Roughened Walls.

As shown in Figure 38, the empirical data fits extremely well to the theoretical curve for the QFFM for most of the measured data (Nikuradze's r/k values shown). The fit is not so good at the higher relative roughness values due to deficiencies in the experimental procedure as acknowledged in the original publication by Nikuradze himself.

Note that in our Figure 38 herein, we show no data extending into the laminar flow region at low values of Q_N . This is because we cannot find within the four corners of Nikuradze's publication any measurements taken at low Reynolds numbers. In Figure 9 of the original paper on page 6, written in German, Nikuradze's plot shows a straight line

through the laminar region connected to the turbulent region by the now famous "dip/rise" in the line, the so-called "Nikuradze inflection profile". We believe that these plotted points on the graph were added by Nikuradze to make it appear as though his roughened data was a continuation of the conventional wisdom for laminar flow, but that it did not represent any of the experimental measurements reported in his paper.

Conventional folklore concerning the so-called "Nikuradze inflection profile" is awash with hysteria and, the scientific literature is inundated with replicas of Nikuradze's Figure 9 plot [43, 44], as well as fake replicas of the plot, mostly by

mathematicians, who have used advanced mathematical algorithms in misguided attempts to rationalize Nikuradze's supposed measurements connecting the laminar and fully turbulent regions of the flow regime [45]. *The reality is that Nikuradze never measured any such inflection point.* He is guilty of supplementing his *measured data* using roughened pipes in the fully turbulent regime with *theoretically projected* dogma relating to the laminar flow regime, *on the same plot*, without ever articulating the different origins of the plotted data.

We also found a discrepancy of a factor of 1,000 in the units of pressure drop data reported in the tables of data in

the original paper. We cannot be sure of where this error came from, but it is conceivable that it was simply a unit conversion error made by Nikuradze in preparing the manuscript for publication.

We digress here to explain the true nature of the transition from the so-called laminar to the fully turbulent flow regime using the QFFM. As shown in Figure 39 below, we show that in our worked example for a packed conduit, there is a well-defined profile, free of any inflection or other disturbance, for relative roughness coefficients in the range of $0 \leq k_{dc} \leq 0.5$, which corresponds to values of $1 \leq \lambda \leq 25$. This range encompasses *all* of Nikuradze's roughened data.

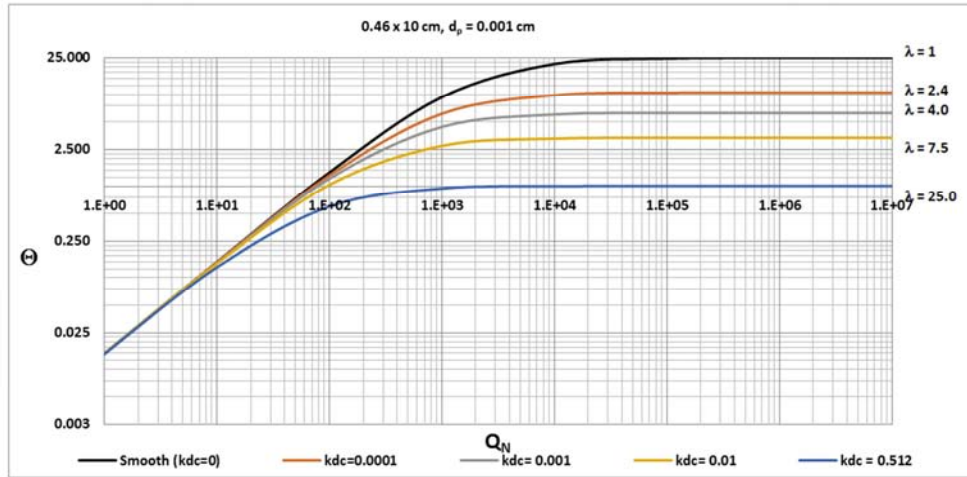


Figure 39. Packed Conduit.

Because the primary wall effect is negligible in the packed column of our worked example, the boundary layer is infinitesimally thin, even at low values of Q_N , which establishes the baseline for the entire fluid flow regime ($\omega_0=1/8\pi$, the base frequency of the harmonic oscillator). By comparison, as shown also in Figure 39, the overlay of our worked example for the corresponding smooth-walled empty conduit, $k_{dc}=0$, we can see that even though there is a significant primary wall effect, the boundary layer, which is

initially very significant, gradually dissipates at higher values of Q_N , but does so in a very *controlled* manner, also without any inflection or other disturbances in the profile.

Additionally, as shown in Figure 40 below for the corresponding empty conduit, we can see that, in contrast to the packed column, even though the boundary layer *delays* the impact of the wall roughness as a function of Q_N , it does so in a very gradual well-defined manner without any inflection or other points of discontinuity.

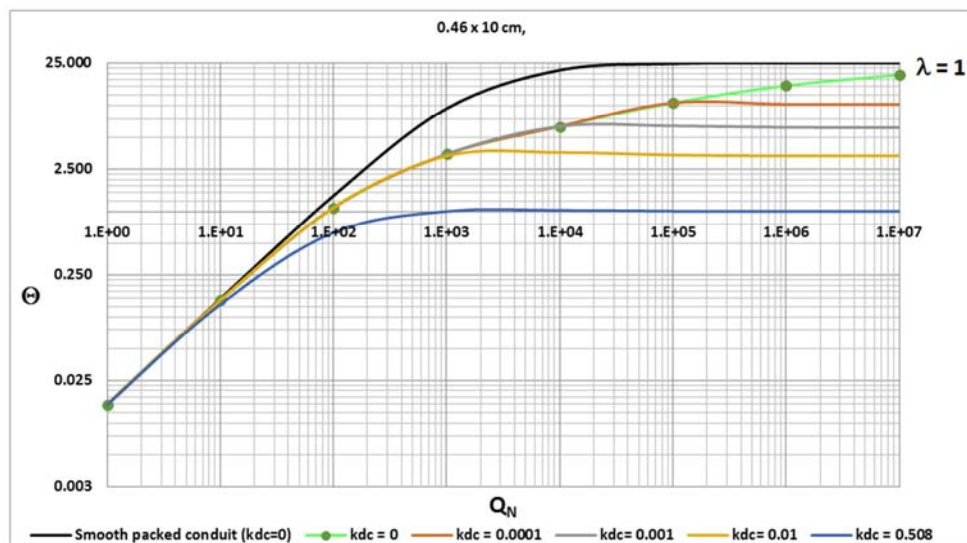


Figure 40. Empty Conduit.

Importantly, as shown in Figure 41 below, when we overlay both portions of Nikuradze's measurements, i.e. the smooth and roughened pipe data, with our worked example for an empty conduit, we can see the orderly progression from the so-called laminar regime, where smooth and roughened pipes are indistinguishable due to the impact of

the boundary layer, to the so-called fully turbulent regime, where roughened pipe data deviates from smooth walled data according to the value of λ , which is due to the overall net wall effect. The line for $\lambda=1$ is shown in the plot as a reference marker.

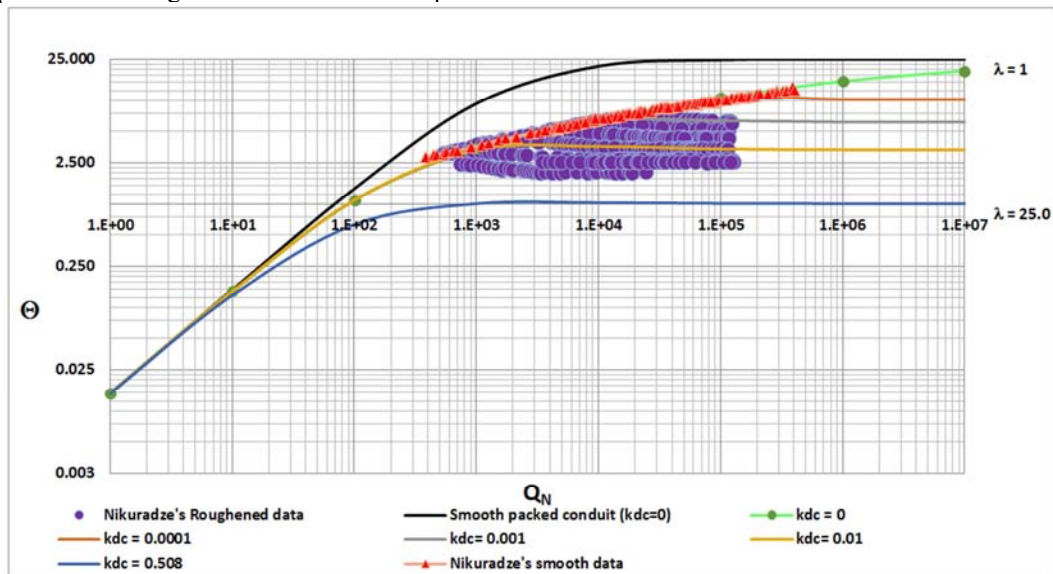


Figure 41. Nikuradze Smooth & Roughened Overlay of Empty Conduit.

Accordingly, in direct contrast to the “Nikuradze inflection profile” enthusiasts, we dismiss *in its entirety* any notion that there is a “discontinuity” in the fluid current as the fluid flow rate accelerates from rest to exceedingly large values.

5.5. All Conduits in the Same Frame of Reference

Finally, a major benefit of the QFFM is that we can view

all the experimental data used in our validation protocol for both packed and empty conduits in the same frame of reference.

Firstly we view the entire validation data as a plot of Θ versus Q_N , in Figure 42 below.

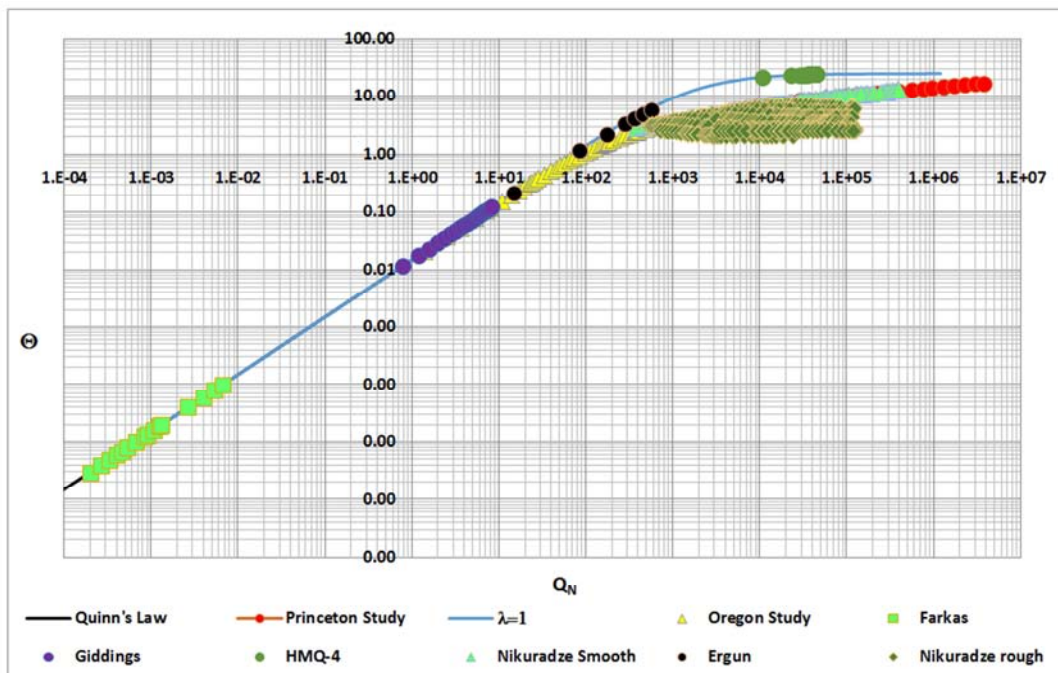


Figure 42. QFFM Validation-Closed Conduits.

As shown in Figure 42, this frame of reference differentiates between packed and empty conduits, on the one hand, and between smooth and roughened walls, on the other.

Alternatively, we can view the entire validation data in the linear format of Quinn's Law, as a plot of P_Q versus C_Q , as shown in Figure 43 below.

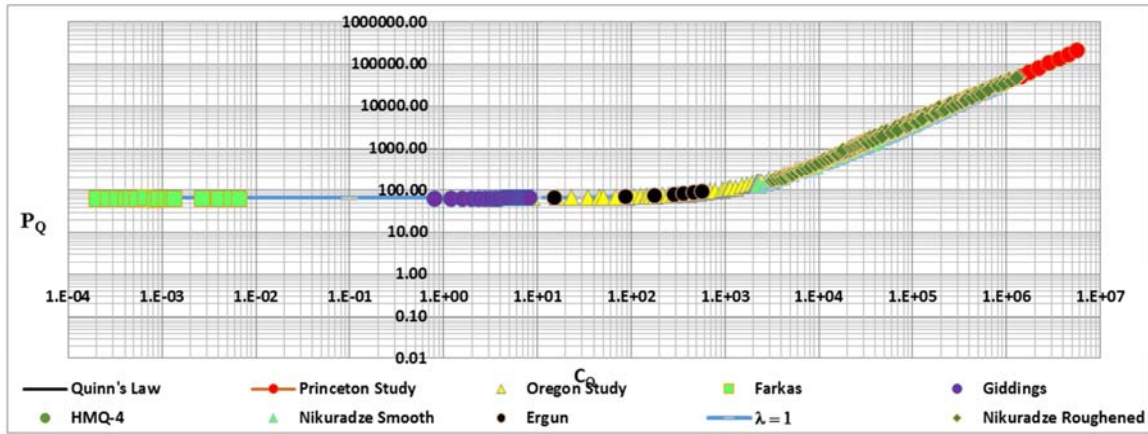


Figure 43. Quinn's Law Validation-Closed Conduits.

As shown in Figures 42 and 43, the regions of the *subjective* fluid flow regime, i.e. laminar, transitional and turbulent, are clearly marked on the x axis. We do *not* suggest that the ranges of values of Q_N are accurate for each of these designated regimes of flow, since we contend that these labels are of “*qualitative*” value *at best*. The plot is log-log to facilitate the data points for both packed and empty conduits over an extremely wide range of modified Reynolds numbers, and all of which fall on a straight line of slope $1/(8\pi)$ and intercept $64\pi/3$.

The QFFM, therefore, teaches that *every experiment* carried out in a closed conduit, whether packed with solid particles or devoid of solid particles (a capillary or empty conduit), must fall on the straight line shown in Figure 43. Thus, this teaching removes *all* ambiguity in the pressure/fluid flow relationship in closed conduits and, in addition, defines *precisely* the role of each flow embodiment parameter as well as that of the flowing fluid. The only source of error remaining is related to the *accuracy* of a

particular *measurement technique*, i.e., where *exactly* on the line a particular experimental result should fall.

Accordingly, for the *first* time in the history of fluid dynamic experiments, the only arguments, which are valid pertaining to fluid flow in closed conduits, are those which are related to the *precise value* of the particular measured parameters, *not* the *fundamentals* underlying the relationship between the *driving force* (ΔP) and the resultant *flow rate* (q).

6. Model Comparisons

In the interest of quantifying the QFFM relative to other conventional flow models, we include a comparison to the Poiseuille [46] and Blasius [47] models in the QFFM frame of reference, shown below in Figure 44. The Poiseuille model pertains to the laminar region and the Blasius model is supposed to be accurate over some specified narrow region of the turbulent regime.

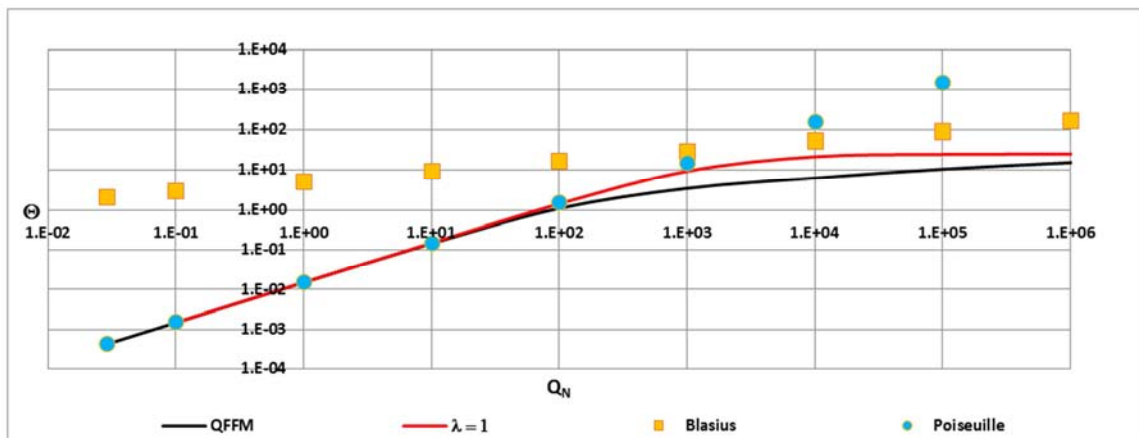


Figure 44. Comparison of QFFM, Blasius and Poiseuille.

As shown in Figure 44, the QFFM and the Poiseuille models are very closely matched at low values of Q_N , the

region in which the Poiseuille model is generally regarded as being valid. The Blasius model, on the other hand, completely misses the mark across the entire region of the flow regime. It is off by an order of magnitude in the *wrong* direction at its closest point to the QFFM, which, curiously, falls in the transitional region of the flow regime, i.e., the region of the flow regime corresponding to the so-called “Nikuradze inflection profile”. Accordingly, we suggest that the Blasius model is virtually worthless.

7. Conclusions

As of this writing, the Navier-Stokes equation for fluid flow stands without analytical solution. We do not say if this is because the currently accepted/popular theories of fluid flow in closed conduits are fatally flawed, or because the equation itself is *necessarily* deficient.

In this paper, we have derived a unique theory of fluid flow in closed conduits. We do not claim that our theory provides a “solution” to the Navier-Stokes equation *per se*, but we feel confident that it correctly and uniquely describes fluid flow in closed conduits.

Probably the most important disclosure herein, relative to conventional wisdom, is that the conventional Reynolds number, by itself, is *inadequate* to define kinetic contributions to overall conduit permeability. In its place, we have defined the “fluid current” as the *governing kinetic parameter* which incorporates *all* contributing elements to the fluid flow regime.

In addition, and with almost equal implications, the concept of “chaotic flow profile” has been shown herein to be unfounded. Instead, we have provided a predictable and structurally stable, pattern of fluid flow profile, which is directly related to the fluid flow embodiment and instantaneous operating conditions in any given experiment under study.

Finally, this paper puts to rest, once and for all, the *myth* that packed and empty conduits belong to two *different* flow regimes. On the contrary, it is now clear that both are governed by the exact same Laws of Nature.

Acknowledgements

I wish to acknowledge Eugene M Van loan III for discussions on this subject matter for more than 20 years. In addition, I also want to acknowledge Hubert M Quinn Jr., my son, for his engineering contribution in designing a continuous fluid flow loop, which enables visualization of many of the underlying concepts described in this paper.

References

- [1] H. Darcy, Les Fontaines Publiques de la Ville de Dijon, Victor Dalmont, Paris, France, 1856.
- [2] E. Erdim, O. Akgiray, I. Demir; A revisit of pressure drop-flow rate correlations for packed beds of spheres, *Powder Technology* 283 (2015) 488-504.
- [3] N. Dukhan, O. Bagci, M. Ozdemir. Experimental flow in various porous media and reconciliation of Forchheimer and Ergun relations. *Experimental Thermal and Fluid Science* 57 (2014) 425-433.
- [4] CHARLES L. FEFERMAN, EXISTENCE AND SMOOTHNESS OF THE NAVIER-STOKES EQUATION <http://www.claymath.org/sites/default/files/navierstokes.pdf>.
- [5] H. M. Quinn, J. J. Takarewski, E. Williams, US 7,767,463, Method for screening mobile phases in chromatography systems (2010).
- [6] H. M. Quinn, J. E. Brann, III, US 6,149,816, Chemical analyses (2000).
- [7] H. M. Quinn, John E. Brann, III, US 6,110,362, Chemical analyses (2000).
- [8] H. M. Quinn, R. A. Menapace, C J. Oberhauser, US 5,968,367, High performance liquid chromatography method and apparatus (1999).
- [9] H. M. Quinn, J. J Takarewski, US 5,919,368, High performance liquid chromatography method and apparatus (1999).
- [10] H. M. Quinn, R. A. Menapace, C J. Oberhauser US 5,795,469, High performance liquid chromatography method and apparatus (1998).
- [11] H. M. Quinn, J. J. Takarewski, US 5,772,874, High performance liquid chromatography method and apparatus (1998).
- [12] H. M. Quinn, US 20100071444, Throughput Screening, Purification and Recovery System for Large and Small Molecules (2010).
- [13] G. Guiochon, S. G. Shirazi, and A. M. Katti, Fundamentals of Preparative and Nonlinear Chromatography, Academic Press, Boston, Mass, USA, 1994.
- [14] R. Endeke, I. Halasz, and K. Unger, *J. Chromatography*, 99, 377 (1974).
- [15] D. Cabooter, J. Billen, H. Terryn, F. Lynen, P. Sandra, G. Desmet; *Journal of Chromatography A*, 1178 (2008) 108–117.
- [16] F. Gritti, D. S. Bell, G. Guiochon; *Journal of Chromatography A*, 1355 (2014) 179–192.
- [17] Kim Vanderlindena, Gert Desmeta, David S. Bellb, Ken Broeckhoven, Detailed efficiency analysis of columns with a different packing quality and confirmation via total pore blocking, *Journal of Chromatography A*, 1581–1582 (2018) 55–62.
- [18] U. Neue, HPLC Columns-Theory, Technology and Practice, Wiley-VCH, 1997.
- [19] A. E. Reising, J. M. Godinho, K. Hormann, J. W. Jorgenson, U. Tallarek. Larger voids in mechanically stable, loose packings of 1.3 mm frictional, cohesive particles: Their reconstruction, statistical analysis, and impact on separation efficiency: *Journal of Chromatography A*, 1436 (2016) 118-132.
- [20] P. C. Carman, “Fluid flow through granular beds,” *Transactions of the Institution of Chemical Engineers*, vol. 15, pp. 155–166, 1937.

- [21] R. B. Bird, W. E. Stewart, and E. N. Lightfoot, *Transport Phenomena*, John Wiley & Sons, 2002.
- [22] Dejan Brkić and Pavel Praks, Unified Friction Formulation from Laminar to Fully Rough Turbulent Flow; *Appl. Sci.* 2018, 8, 2036; doi: 10.3390/app8112036.
- [23] M. Rhodes, *Introduction to Particle Technology*, John Wiley & Sons, 1998.
- [24] L. Prandtl, in *Verhandlungen des dritten internationalen Mathematiker-Kongresses in Heidelberg 1904*, A. Krazer, ed., Teubner, Leipzig, Germany (1905), p. 484. English trans. in *Early Developments of Modern Aerodynamics*, J. A. K. Ackroyd, B. P. Axcell, A. I. Ruban, eds., Butterworth-Heinemann, Oxford, UK (2001), p. 77.
- [25] K. E. Bullen, *An Introduction to the Theory of Mechanics*, 7th edition, Cambridge AT THE UNIVERSITY PRESS 1965.
- [26] J. C. Giddings, *Dynamics of Chromatography, Part I: Principles and Theory*, Marcel Dekker, New York, NY, USA, 1965.
- [27] J. C. Giddings, *Unified Separation Science*, John Wiley & Sons, 1991.
- [28] K. B. SOUTHERLAND, R. D. FREDERIKSEN, W. J. A. DAHM; Comparisons of Mixing in Chaotic and Turbulent Flows; *Chaos, Solitons & Fractals* Vol. 4, No. 6, pp. 1057-1089, 199.
- [29] T. Farkas, G. Zhong, G. Guiochon, Validity of Darcy's Law at Low Flow Rates in Liquid Chromatography *Journal of Chromatography A*, 849, (1999) 35-43.
- [30] H. M. Quinn; A Reconciliation of Packed Column Permeability Data: Column Permeability as a Function of Particle Porosity *Journal of Materials* Volume 2014 (2014), Article ID 636507, 22 pages <http://dx.doi.org/10.1155/2014/636507>.
- [31] J. M. Coulson; University of London, Ph. D. thesis, "The Streamline Flow of Liquids through beds comprised of Spherical particles" 1935.
- [32] Ergun, S. and Orning, A. A., Fluid Flow through Randomly Packed Columns and Fluidized Beds, *Ind. Eng. Chem.* vol. 41, pp. 1179, 1949.
- [33] Ergun, S., Determination of Particle Density of Crushed Porous Solids, *Anal. Chem.* vol. 23, 1951.
- [34] Ergun, S., Fluid Flow Through Packed Columns, *Chem. Eng. Progr.* vol. 48, pp. 89-94, 1952.
- [35] H. M. Quinn, A Reconciliation of Packed Column Permeability Data: Deconvoluting the Ergun Papers *Journal of Materials* Volume 2014 (2014), Article ID 548482, 24 pages <http://dx.doi.org/10.1155/2014/548482>.
- [36] H. M. Quinn, Reconciliation of packed column permeability data—part 1: the teaching of Giddings revisited, *Special Topics & Reviews in Porous Media*, vol. 1, no. 1, pp. 79–86, 2010.
- [37] B. J. McKeon, C. J. Swanson, M. V. Zagarola, R. J. Donnelly and A. J. Smits. Friction factors for smooth pipe flow; *J. Fluid Mech.* (2004), vol. 511, pp. 41-44. Cambridge University Press; DOI; 10.1017/S0022112004009796.
- [38] B. J. McKeon, M. V. Zagarola, and A. J. Smits. A new friction factor relationship for fully developed pipe flow; *J. Fluid Mech.* (2005), vol. 238, pp. 429-443. Cambridge University Press; DOI; 10.1017/S0022112005005501.
- [39] C. J. Swanson, B. Julian, G. G. Ihas, and R. J. Donnelly. Pipe flow measurements over a wide range of Reynolds numbers using liquid helium and various gases. *J. Fluid mech.* (2002), vol. 461, pp. 1-60. Cambridge University Press; DOI; 10.1017/S0022112002008595.
- [40] J. Nikuradze, NASA TT F-10, 359, *Laws of Turbulent Flow in Smooth Pipes*. Translated from "Gesetzmäßigkeiten der turbulenten Stromung in glatten Rohren" VDI (Verein Deutscher Ingenieure)-Forschungsheft 356.
- [41] H. M. Quinn, Unpublished data.
- [42] j. Nikuradze, NACA TM 1292, *Laws of Flow in Rough Pipes*, July/August 1933. Translation of "Stromungsgesetze in rauhen Rohren." VDI-Forschungsheft 361. Beilage zu "Forschung auf dem Gebiete des Ingenieurwesens" Ausgabe B Band 4, July/August 1933.
- [43] M. DOBRNJAC, DETERMINATION OF FRICTION COEFFICIENT IN TRANSITION FLOW REGION FOR WATERWORKS AND PIPELINES CALCULATION, MECHANICAL ENGINEERING FACULTY, UNIVERSITY IN BANJALUKA, BANJALUKA, REPUBLIC SRPSKA, BOSNIA & HERZEGOVINA.
- [44] A. Ramakrishna Rao, B. Kumar, Friction Factor for Turbulent Pipe Flow, Department of Civil Engineering, IISc, Bangalore-560012, India.
- [45] B. H. Yang, D. D. Joseph, Virtual Nikuradse, *Journal of Turbulence* Vol. 10, No. 11, 2009, 1–28.
- [46] J. L. M. Poiseuille, *Memoires des Savants Etrangers*, Vol. IX pp. 435-544, (1846); BRILLOUIN, M. (1930) Jean Leonard Marie Poiseuille. *Journal of Rheology*, 1, 345.
- [47] H. Blasius (1908). "Grenzschichten in Flüssigkeiten mit kleiner Reibung". *Z. Angew. Math. Phys.* 56: 1–37.